Applied Thermal Engineering 221 (2023) 119847

Contents lists available at ScienceDirect

Applied Thermal Engineering

journal homepage: www.elsevier.com/locate/apthermeng

Research Paper

Pore-scale analysis of two-phase nanofluid flow and heat transfer in open-cell metal foams considering Brownian motion

Hamidreza Khoshtarash [a], Majid Siavashi [a,*], Milad Ramezanpour [a], Martin J. Blunt [b]

[a] Applied Multi-Phase Fluid Dynamics Laboratory, School of Mechanical Engineering, Iran University of Science and Technology, Tehran, Iran
[b] Department of Earth Science and Engineering, Imperial College London, London SW7 2AZ, United Kingdom

ARTICLE INFO

Keywords:
Porous media
Pore-scale modeling
Open-cell metal foam (OCMF)
Nanofluid
Buongiorno's model
Brownian motion

ABSTRACT

Simultaneous use of porous media and nanofluids will increase the convective heat transfer multiple times compared to non-porous and pure fluid conditions. Heat transfer and flow transport of nanofluids inside porous media are usually simulated in large-scale with average properties, which are typically highly uncertain. Pore-scale simulation as an alternative approach can capture the characteristics of flow and heat transfer more accurately. Only few studies have been conducted to study nanofluid flow through porous media in pore-scale, and most of them employed single-phase approach without focus on different affective forces. This paper uses a pore-scale approach to investigate the flow characteristics and convective heat transfer of two-phase nanofluid flow in open-cell metal foams (OCMFs). Simulation of fluid flow and heat transfer is achieved by Buongiorno's model. Therefore, a computational code through the OpenFOAM library that operates by a direct numerical simulation (DNS) approach and the finite volume method (FVM) is used. The momentum, energy, continuity, and nanoparticle distribution equations are discretized, and the SIMPLE algorithm is utilized for pressure and velocity coupling. In the present study, three OCMFs with a constant porosity (0.86) and various pore densities are investigated. Also, variations of pressure gradient, Nusselt number, and Darcy velocity are investigated as a function of pore density (as a geometric parameter), nanoparticle diameter, concentration, and Brownian motion force. The results indicate that the Brownian force enhances the heat transfer in OCMFs from 2% by up to 14% for the nanofluid flowing with 3% nanoparticle concentration. Also, increasing the diameter of nanoparticles reduces the Darcy velocity and heat transfer by up to 4%. On the other hand, increasing particle concentration from 3% to 5%, increases heat transfer by up to 10% and reduces the Darcy velocity by up to 9%. Finally, doubling the pore density demonstrates the complex behavior of the flow patterns, in which the heat transfer increases by up to 30% and permeability and velocity are reduced by up to 70%.

1. Introduction

Heat transfer and fluid flow in porous media have a wide range of theoretical and applied science applications. Some of such applications are oil and gas extraction from petroleum reservoirs [1], new combustion systems with reduced emissions [2], renewable and solar energy systems [3], water resources management [4], underground energy storage [5], thermochemical reactors [6], desalination systems [7], adsorption [8], filtration [9], fuel cells [10,11], drug delivery in biological systems and many more problems [12].

Open-cell foams (OCF) are low-weight porous structures with high permeability, which can be used in various energy systems to improve their performance. Metallic and ceramic OCFs have been used to enhance the thermal and chemical performance of burners [13], heat exchangers [14,15], solar collectors [16], thermal energy storage units [17,18], and chemical reactors [19]. For instance, in an experimental study on shell and tube thermal energy storage units, the pattern of annular porous fins is optimized [20]. Also, the melting process is studied in another investigation on a thermal energy storage unit filled with open-cell metal foams (OCMFs) [21]. It was demonstrated that the melting time is considerably dependent on the geometrical parameters of the OCMFs, such as the pore density. Busser et al. [22] experimentally investigated the hydrodynamics and heat transfer of two-phase flows (gas-liquid) with different flow regimes in a thin sheet of highly porous OCF.

Numerical simulation is a common tool to analyze transport phenomena in porous media. Darcy-scale or macro-scale analysis of porous

* Corresponding author.
E-mail address: msiavashi@iust.ac.ir (M. Siavashi).

https://doi.org/10.1016/j.applthermaleng.2022.119847
Received 16 July 2022; Received in revised form 25 November 2022; Accepted 8 December 2022
Available online 13 December 2022

Nomenclature

c_p	Specific heat capacity, (J kg^{-1} K^{-1})
d	Molecule diameter, (m)
d_p	Pore diameter, (m)
D_B	Brownian coefficient, m^2s^{-1}
h	Overall heat transfer coefficient, W/m^2K
$\overrightarrow{J}$	Mass flux, ($kg\,m^2\,s^{-1}$)
$\boldsymbol{J_p}$	Nanoparticle diffusion mass flux, ($kg\,m^2\,s^{-1}$)
k	Thermal conductivity, ($Wm^{-1}k^{-1}$)
$\boldsymbol{K}$	Permeability tensor, (m^2)
k_B	Boltzmann's constant, (Jk^{-1})
$\boldsymbol{K_D}$	Darcy permeability tensor, (m^2)
$\boldsymbol{K_F}$	Forchheimer permeability tensor, (m^2)
L	Sample length, (m)
$\dot{m}$	Mass flow rate, ($kg\,s^{-1}$)
Nu_d	Nusselt number
p	Pressure, (Pa)
T	Temperature, (K)
$\overline{T}$	Average temperature, (K)
T_{in}	Inlet fluid temperature, (K)
T_w	Inlet Wall Temperature, (K)
$(T_w)_{inlet}$	Outlet wall temperature, (K)
$(T_w)_{outlet}$	Outlet wall temperature, (K)
q''	Heat flux, (Wm^{-2})
Re_k	Reynolds number, ($\rho U K_D^{1/2}/\mu$)
$\boldsymbol{U}$	Darcy velocity, ($m\,s^{-1}$)
$\boldsymbol{V}$	Velocity, ($m\,s^{-1}$)
∇p	Pressure gradient, ($Pa\,m^{-1}$)

Greek Symbols

ε	Porosity
ρ	Density, $kg\,m^{-3}$
μ	Dynamic viscosity, ($kg\,m^{-1}\,s^{-1}$)
β	Thermal expansion coefficient, (K^{-1})
β_F	Forchheimer coefficient,
φ	Nanoparticles' volume fraction,
ν	Kinematic viscosity, (m^2s^{-1})

Subscripts

$\boldsymbol{B}$	Brownian Motion
D	Darcy
F	Forchheimer
eq	Equivalent
i	Nanoparticle's moving direction
f	Fluid
in	Inlet
out	Outlet
nf	Nanofluid
np	Nanoparticle
p	Porous
s	Solid

Acronyms

OCF	Open-cell foam
OCMF	Open-cell metal foam
CAD	Computer-aided design
FVM	Finite volume method
WP	Weaire–Phelan
PNM	Pore-network modeling
PPI	Pores per inch
STL	Standard triangle language

media is traditionally used to investigate such problems. However, this method of analysis necessitates characterization of the porous medium to extract its average properties, such as the Forchheimer coefficient, onset of the non-Darcy regime, permeability, and overall heat transfer coefficient. These properties can be obtained from experimental investigations, which are expensive. In contrast, pore-scale numerical analysis can aid us in characterizing porous media to perform macro-scale analyses. The results can be used to suggest improved designs of porous materials. In pore-scale analysis, a detailed geometry of pores is generated, and the governing equations are solved in the pore structure. Pore-scale analysis can be done through two techniques: 1- pore network modeling (PNM) and 2- direct numerical simulation (DNS). In the first method, a simplified pore-network model represents the detailed porous structure, and analytical relations are used to resolve the governing equations in pores and throats. While in the second method, the governing equations are solved numerically on the original pore-scale geometry [23]. In the past two decades, much research have been done on pore-scale imaging and numerical simulation. Raeini et al. [24] studied a new approach of PNM for multiphase flow in a mixed-wet and water-wet reservoir. Their results showed that flow characteristics and image processing algorithm parameters introduce an enormous difference in the calculations of upscaled flow properties. Numerical methods have been developed to perform DNS and resolve various physics in pore-scale. The finite volume method (FVM) is a powerful numerical technique which is commonly used to solve problems in complex geometries. Ramezanpour et al. [25] used the DNS method to investigate nanoparticles' deposition in a microchannel by pore-scale approach.

Most DNS studies are confined to multiphase flows (in absence of thermal analysis) in low-permeability porous rocks, which are used in the petroleum industry. A few studies have been done on open-cell porous foams to characterize their hydro-thermal properties. Kopanidis et al. [26] studied heat conduction of high porosity metallic OCFs. The study of Moghimi et al. [27] focused on the non-Darcy flow in highly porous structures with different degrees of geometrical complexity. Yao et al. [28] investigated heat transfer in highly porous OCMFs. Trilok and Gnanasekaran [29] computed the flow characteristics and heat transfer rate of OCMFs. They illustrated the performance characteristics of foam samples to enhance heat transfer and curtail flow resistance. These studies are limited to single-phase flows in OCMFs.

Nanofluids –as a slurry of high-conductive nanoparticles and a base fluid– can enhance the heat transfer coefficient. Numerical simulation of nanofluid flow and heat transfer have been the topic of many research studies. The most common approach for nanofluid flow simulation is the single-phase scheme with improved mixture properties [30]. More accurate two-phase simulation approaches such as Eulerian-Eulerian [31,32], Eulerian-Lagrangian [25,33], two-phase mixture [34], and Buongiorno's model [35,36] are also used in this field. Among these models, Buongiorno's equations efficiently and accurately model the most important forces (such as Brownian and thermophoresis) in a nanofluid mixture. Since 2006, this method has been used for the numerical simulation of nanofluids in different problems. The use of nanofluid flowing through a highly conductive OCF has been the subject of many recent investigations. For systems employing nanofluids and porous media, studying the hydraulic and thermal parameters is essential [37]. Heat transfer problems with free [38,39], forced [40,41], or mixed convection [42,43] mechanisms have been analyzed in various geometries [44]. The main conclusion of these research works is that simulateneous applying porous foams and nanofluid can substantially improve heat transfer at the expense of a minor increment in pressure loss and pumping power. For instance, Yekani motlgh et al. [45] studied

Table 1
Comparison of the most recent studies about nanofluid flow through porous media.

Authors	Method of solution	Scale	Assumptions
Sheremet and Pop [46]	Finite difference method	Large-scale approach	Two-phase flow-Heat transfer
Yekani Motlagh et al. [47]	Finite volume method	Large-scale approach	Two-phase flow-Heat transfer
Habibi Matin and Pop [42]	Analytical method	Large-scale approach	Two-phase flow-Heat transfer
Dickson et al. [43]	Analytical method	Large-scale approach	Two-phase flow-Heat transfer
Malvandi et al. [48]	Finite volume method	Large-scale approach	Two-phase flow-Heat transfer
Malvandi et al. [49]	Finite volume method	Large-scale approach	Two-phase flow-Heat transfer
Fazeli et al. [40]	Finite volume method	Large-scale approach	Two-phase flow-Heat transfer
Selimefendigil and Oztop [50]	Finite volume method	Large-scale approach	Two-phase flow-Heat transfer
Sheikholeslami [52]	CVFEM method	Large-scale approach	Two-phase flow-Heat transfer
Hatami et al. [54]	Finite Element Method	Large-scale approach	Two-phase flow-Heat transfer
Andarwa et al. [55,56]	Eulerian-Lagrangian method	Pore-scale approach (microchannel)	Two-phase flow
Seetha et al. [57]	Eulerian method	Pore-scale approach (microchannel)	Two-phase flow
Ramezanpour et al. [25]	Eulerian-Lagrangian method	Pore-scale approach (microchannel)	Two-phase flow
Su et al. [61]	Eulerian-Lagrangian method	Pore-scale approach (porous media)	Two-phase flow
Moghimi et al. [27]	Eulerian method	Pore-scale approach (porous media)	One-phase flow
Poureslami et al. [64]	Eulerian method	Pore-scale approach (porous media)	One-phase flow-Heat transfer
Sepehri and Siavashi [62]	Eulerian method	Pore-scale approach (porous media)	One-phase flow-Heat transfer
Minakov et al. [59]	volume of fluid (VOF) method	Pore-scale approach (porous media)	Two-phase flow
Buonomo et al. [63]	Eulerian method	Pore-scale approach (porous media-Kelvin cell)	Two-phase flow-Heat transfer

the two-phase flow of nanofluids inside a porous-semi annulus cavity with the Buongiorno's approach. Their results indicated that increasing the volume fraction of nanofluids enhances the Nusselt number. Sheremet and Pop [46] investigated Darcy–Boussinesq model in the porous cavity by considering Brownian diffusion and thermophoresis. They demonstrated that the heat transfer was enhanced, and convection flow was reduced by decreasing the distance between the vertical wall and the heat source. In another study, Yekani Motlagh et al. [47] employed Buongiorno's model with Brownian motion and thermophoresis effects. Their results indicated that the thickness of the mass boundary layer reduced with the decrement of the porosity. Malvandi et al. [48] studied thermal performance of the nanofluid in a circular microchannel by considering Brownian motion and thermophoresis, numerically. In another study by Malvandi et al. [49], the nanoparticle transport phenomenon was considered in Buongiorno's model. Selimefendigil and Oztop [50] worked on heat transfer and flow characteristics in a U-shaped porous channel under the effect of magnetic fields. Siavashi et al. [51] investigated the two-phase nanofluid model by using Darcy-Brinkman- Forchheimer's relation in porous media in a large-scale approach. Their results demonstrated the optimum thickness of porous layers in partial filling in which heat transfer maximizes. Sheikholeslami [52] studied the effect of the Lorentz forces on the natural convection of nanofluid in the porous cavity. The results show that the heat transfer

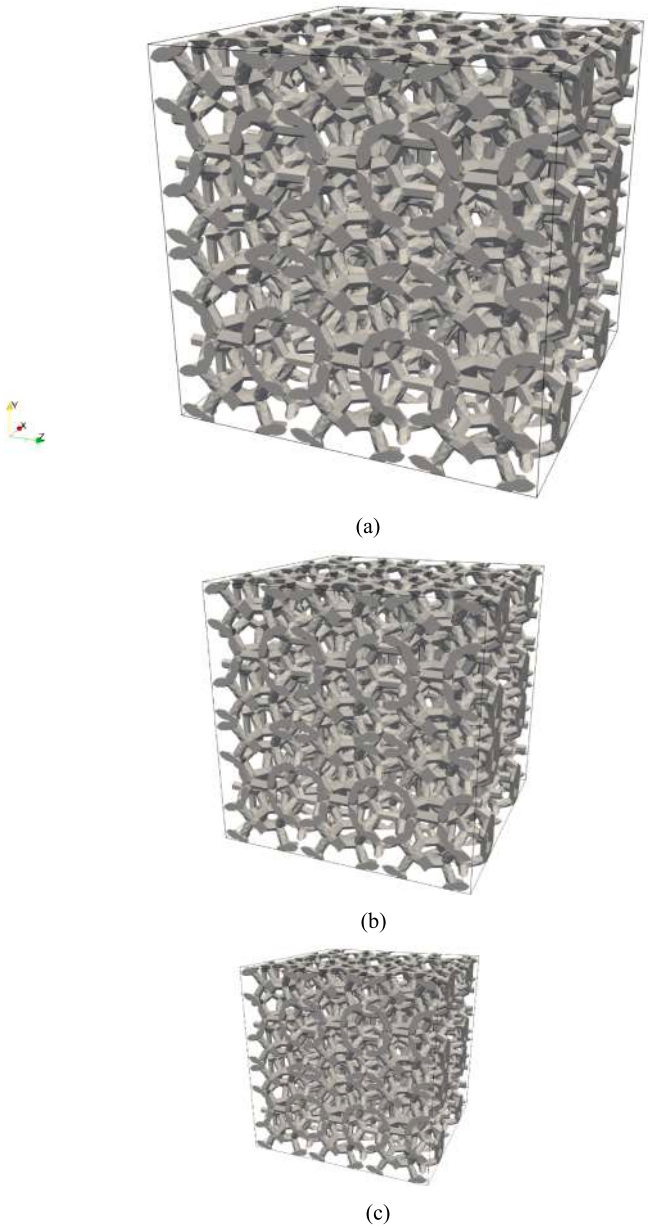

Fig. 1. Geometry of three OCF samples with a porosity of 0.86. (a), (b), and (c) are samples 1,2, and 3, respectively.

Table 2
Physical properties of the open-cell foam samples studied in this work.

Sample number	Porosity	Dimensions (mm^3)	Pore diameter (mm)	Pore density (PPI)	Ligament diameter (mm)
1	0.86	$6 \times 6 \times 6$	1.270	20	0.192
2	0.86	$4 \times 4 \times 4$	0.847	30	0.133
3	0.86	$3 \times 3 \times 3$	0.635	40	0.096

Table 3
Thermophysical properties of the nanoparticles, base fluid, and metallic OCF used in the simulations.

Material	$\mu[mPa.s]$	$\rho[kg.m^{-3}]$	$\lambda[W.m^{-1}K^{-1}]$	$cp[J.kg^{-1}K^{-1}]$
Base fluid (water)	0.7972	995.7	0.6145	4118
Alumina (Al_2O_3)	–	3.890	40	765
Stainless steel 304A	–	7850	16.5	500

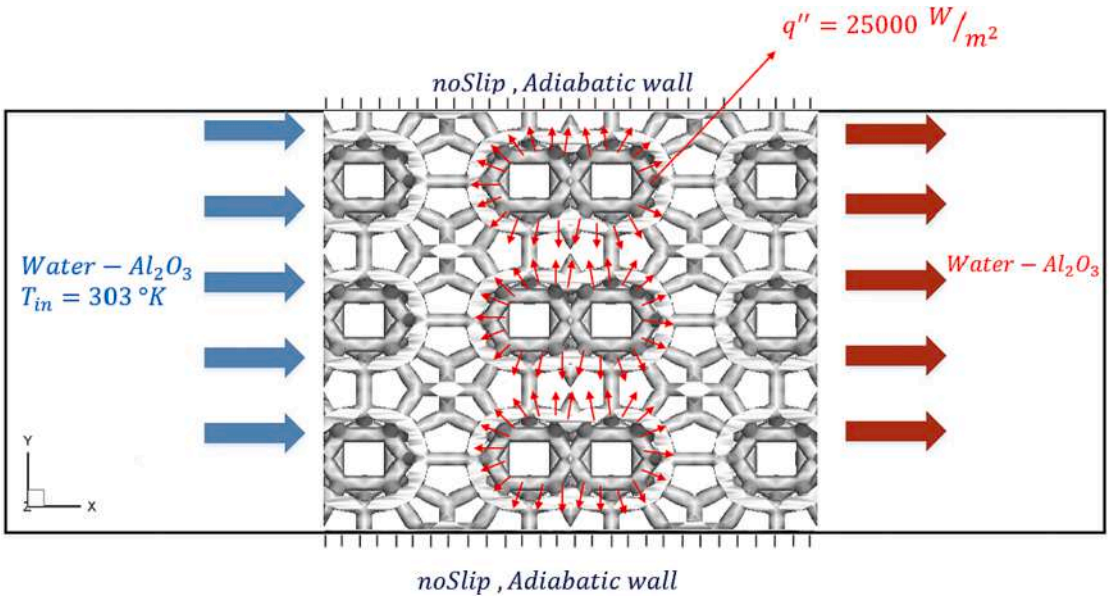

Fig. 2. A schematic representation of boundary conditions for the simulation in an OCF.

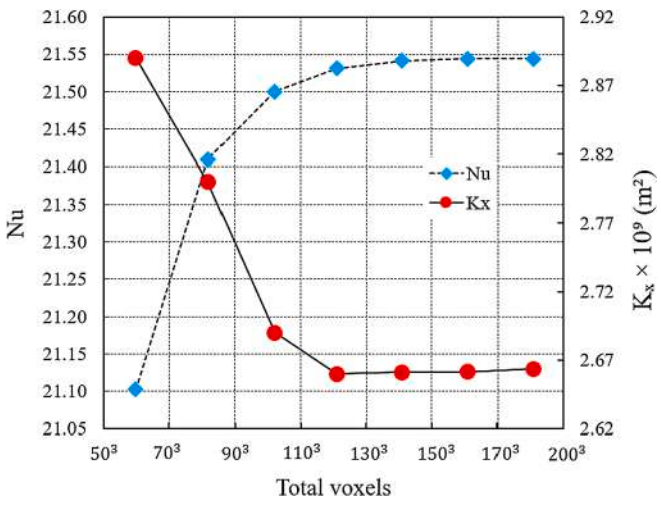

Fig. 3. Mesh dependency analysis of the overall Nusselt number (Nu_d), and the x-direction Darcy permeability (K_x) to the total voxels for sample 3 with the pressure gradient equal to 20 Pa/m.

decreases with enhancing the Hartmann number but increases with increasing the volume fraction of nanofluid. In another study, Heyhat et al. [53] experimentally investigated the effect of nanofluid on the thermal performance of the metal foam as an absorption parabolic trough solar collector. Their study focused on the effect of different volume concentrations on thermal efficiency for different solar absorbers. In another study, Hatami et al. [54] studied the effects of different nanoparticles and porosity of absorber tube on the concentrating parabolic solar collector performance. They investigated the effect of the nanoparticle volume fraction, nanoparticle variety, and Darcy and Rayleigh numbers on the heat and mass transfer. According to their findings, the maximum heat transfer occurs when the volume fractions of nanoparticles and the Rayleigh numbers are at the maximum possible values.

All these research works are conducted with large-scale insight using equivalent porous material properties without considering the porous foam details, which can be far from the real properties of a porous foam. The interaction of nanofluid with the complex structure of porous media is another important point that should be considered in thermo-fluid simulations which could not be observed in these macro-scale works.

A few studies focused on pore-scale simulation of nanofluid flow in simple geometries, representing pore channels such as a microchannel. Andarwa et al. [55,56] studied pore-scale simulation of nanoparticle transport in a microchannel. They utilized the lattice Boltzmann method coupled with Lagrangian particle tracking to study nanoparticle deposition. Seetha et al. [57] conducted pore-scale simulation of nanoparticle transport and deposition in a microchannel. They used Eulerian method to investigate nanoparticle transport.

A few recent studies on nanofluids flowing through porous media have been performed only to study the flow characteristics. These studies analyzed nanofluid flow in porous media to enhance oil recovery or nanofluid flow in oil reservoirs [58]. Minakov et al. [59] investigated the effect of nanofluid on interfacial tension and wettability of two-phase nanofluid flow in a sandstone rock to enhance oil recovery by a pore-scale approach. Zhang et al. [60] experimentally investigated the effects of a nanofluid on the enhancement of oil recovery in carbonates. Su et al. [61] investigated the pore-scale direct numerical simulation of particle transport in porous media. They studied the base point-increment method to enhance the discrete element approach and evaluate particle-particle and particle-wall interactions. Sepehri and Siavashi [62] studied pore-scale simulation of flow and energy transport in a non-Darcy flow regime. They investigated coupled thermo-fluid convection-conduction analyses performed on Laguerre–Voronoi metal foams. In another study, Buonomo et al. [63] investigated the entropy

Table 4
The effect of various grids circumstances on heat transfer and flow results for the three samples.

Sample number	Coarse grid	$K_D[mm^2]$	Nu_d	Medium grid	$K_D[mm^2]$	Nu_d	Fine grid	$K_D[mm^2]$	Nu_d
1	120^3	10.98	14.90	150^3	10.77	14.94	180^3	1.78	14.99
2	100^3	4.98	17.37	120^3	4.80	17.39	140^3	4.78	17.40
3	90^3	2.80	21.41	105^3	2.69	21.50	120^3	2.66	21.54

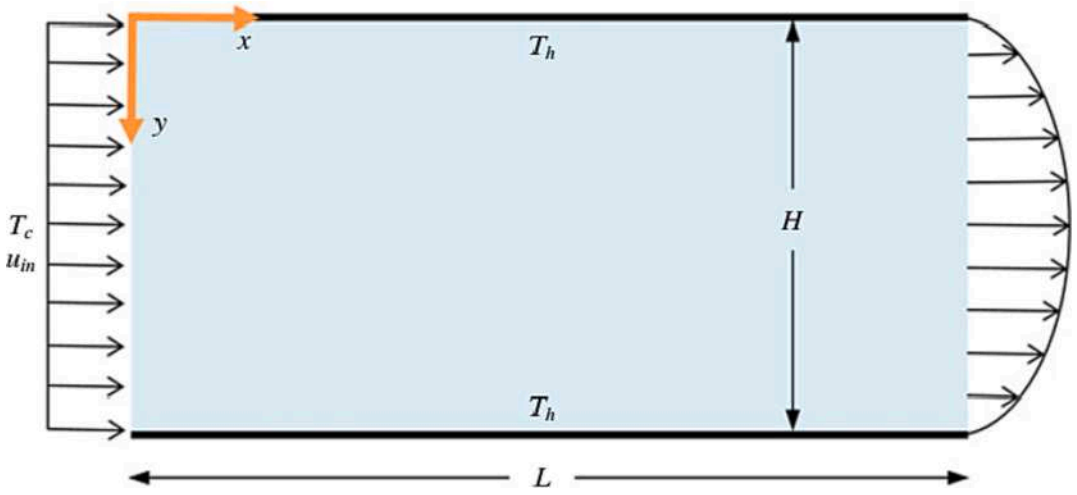

Fig. 4. Nanofluid flow in a microchannel compared to the published results of Sharaf et al. [80].

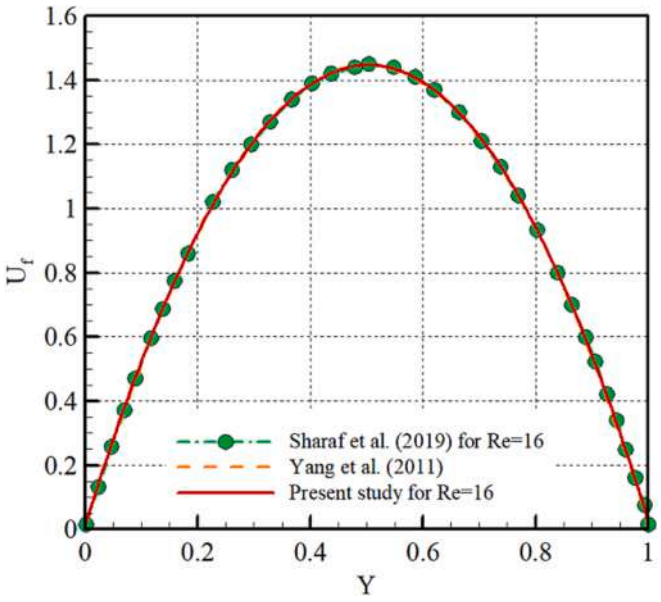

Fig. 5. The non-dimensional velocity profile in the outlet of the microchannel height using the present model and comparing with the results of Sharaf et al. [80], and Yang and Lai [81].

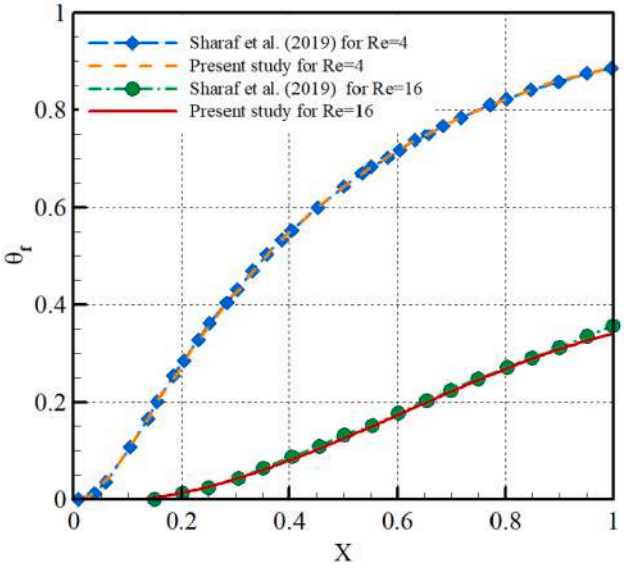

Fig. 6. The non-dimensional temperature profile in the microchannel using the present model and compared with the results of Sharaf et al. [80].

generation of nanofluid in pore-scale.

A summary of the most recent studies considering nanofluid flow through porous media with large-scale and pore-scale insights is listed in Table 1. The above literature survey and the information presented in Table 1 indicate that most recent studies only investigated hydrodynamics and heat transfer of nanofluid flow in large-scale, using averaged properties. Moreover, recent investigations have not investigated the hydro-thermal characteristics of nanofluid flow at the pore-scale. Furthermore, the pore-scale flow analyses through OCFs have been confined to pure fluids or simple geometries, while different influential forces of nanoparticle transport can highly affect the hydro-thermal performance of nanofluid flow through complex porous media.

Based on the mentioned contents, a research gap exists on pore-scale analysis of nanofluid flow in OCFs, considering the most effective nanoparticle transport forces. Interactions of nanofluid and nanoparticles with the complex geometry of the OCF considering different forces could provide more precise insight into different hydro-thermal aspects of nanofluid flow through porous foams, aiding improved process design. Single-phase mixture nanofluid models could not show these effects, while Buongiorno's model can effectively capture such effects. Accordingly, this study investigates the effect of some important influencing parameters of nanofluid on heat transfer and hydrodynamics of a nanofluid slurry flowing through OCFs with different pore densities. The FVM is implemented to resolve the problem, and the three-dimensional (3D) numerical code is developed in the open-source library of OpenFOAM. Weaire–Phelan (WP) foam structures with a constant porosity (0.86) and various pore densities are constructed to perform DNS studies. The nanofluid flow is simulated with Buongiorno's model, and the effect of particle concentration, Brownian motion, nanoparticle diameter, and the pore density of OCFs on hydrodynamics and heat transfer have been thoroughly investigated.

2. Problem statement and mathematical model

2.1. Open-cell foam (OCF) samples

Kelvin and Weaire–Phelan (WP) unit cells are the most widely used structures for OCFs. In this research, the WP structure has been used to

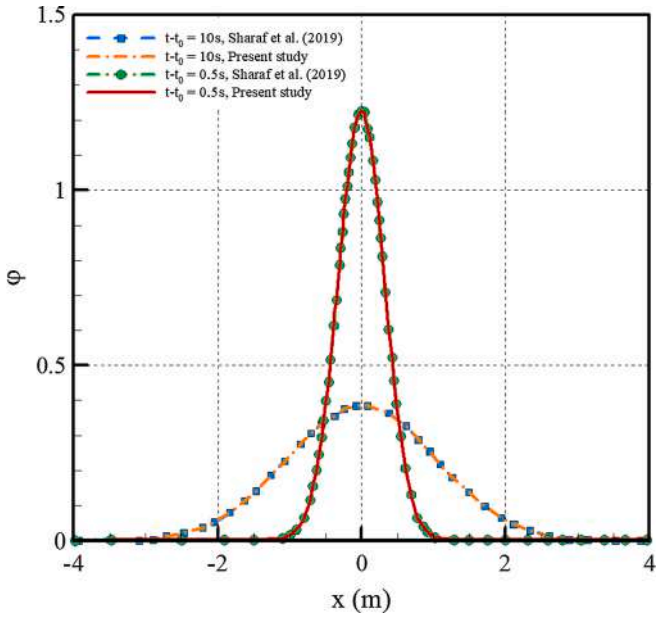

Fig. 7. Nanoparticle concentration profiles for various simulation times using the present model and comparing them with the results of Sharaf et al. [80].

produce OCF samples [65]. The WP structure has irregular hexagons and six tetrahedrons and has been used in many studies [65]. Cunsolo et al. [66] studied hydrodynamics and heat transfer phenomena in Kelvin and Weaire–Phelan structures. They demonstrated that the volumetric Nusselt numbers were almost identical in the two structures when the porosity values were higher than 0.9. However, at a porosity of 0.86, the WP illustrates a better performance. Since the samples used in this study have a porosity of 0.86, the WP structure is selected [65]. This research, employs the same procedure as that of Poureslami et al. [64] to produce OCF samples. As depicted in Fig. 1, three foam samples, having a constant porosity equal to 0.86 with various pore densities (PPI = 20, 30, and 40) are used to conduct simulations. PPI is pores per inch (2.54 cm) and is an inverse representation of pore size. The ligament diameter is the average of all foam, and the ratio of foam diameter to PPI is 25.4. The physical properties of the three samples are summarized in Table 2.

2.2. Problem definition

The effect of Brownian motion, nanoparticle diameter, nanofluid concentration, and foam pore density on the heat transfer and hydrodynamic characteristics of the OCF are analyzed under varying flow conditions. To consider the effect of these parameters, each foam is exposed to different pressure gradients which cover different flow regimes. Parallel simulations are performed on a computational server (Intel® Xeon® processor v2, with 16 threads, 3.3 GHz frequency, and 64 GB memory). Each simulation requires between 10 and 15 h to converge, depending on the number of computational cells and the Reynolds number. Nanoparticles are spherical alumina (Al_2O_3) and the flow is assumed to be incompressible and laminar. Nanofluid enters the domain with atmospheric pressure and a constant temperature of 30℃. The OCF is manufactured from 304A stainless steel, and the thermophysical properties of the nanoparticles, base fluid, and OCMF are given in Table 3.

A schematic of the boundary conditions is presented in Fig. 2. A pressure gradient is imposed across the input–output boundaries to prevent instability in the solutions. This model was proposed by Guo et al. [67]. At the inlet, a constant temperature of 303 K (around the room temperature) is set as the input thermal boundary; surrounding walls have no-slip condition for velocity and are adiabatic. Also, zero mass flux for the volume fraction equation is set at the surface. Heat flux is assumed to be constant and equals 25,000 Wm^{-2} in the interface of the fluid and solid foam, and the no-slip boundary condition, are set at the aforementioned interface.

2.3. Governing equations

The Buongiorno's model explores the heat transfer phenomena caused by seven slip mechanisms: the Magnus effect, Brownian diffusion, fluid drainage, inertia, thermophoresis, gravity, and diffusiophoresis. These mechanisms produce a relative velocity between the base fluid and the nanoparticles. The governing equations as a set of nonlinear ordinary differential equations (ODEs) are solved numerically. Brownian diffusion is among the most important slip mechanisms in nanofluids [68]. Hence, the effect of Brownian motion is investigated in this study.

The governing equations for nanofluid flow obey the Buongiorno's model [68]. The continuity, momentum, nanoparticle distribution, and

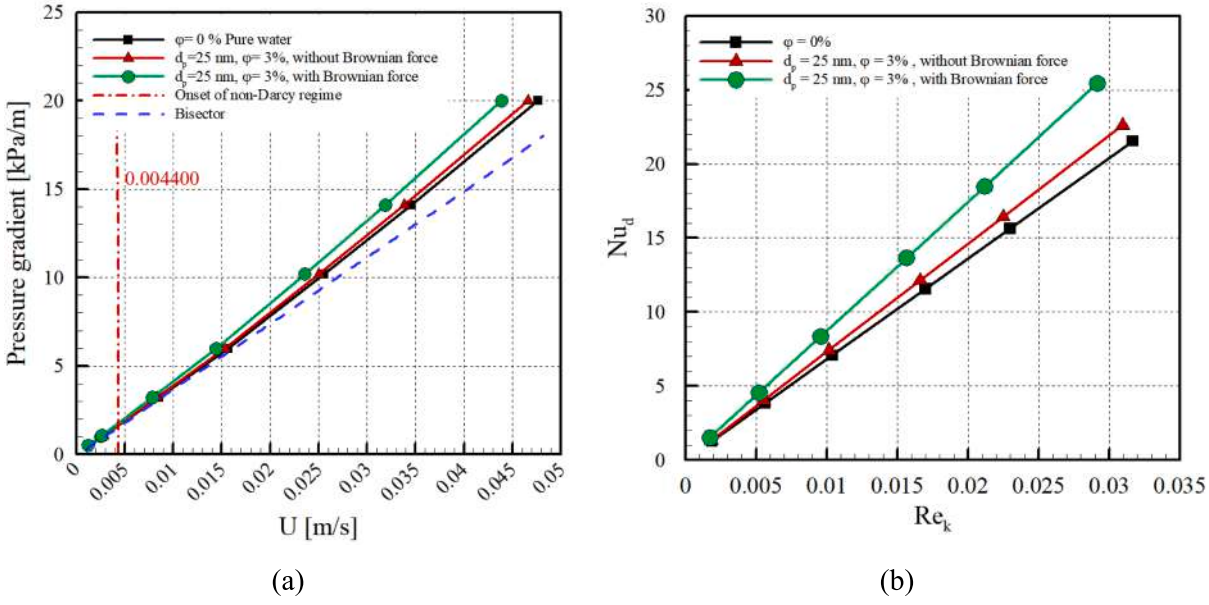

Fig. 8. Brownian motion effects on a) pressure gradient versus the Darcy velocity; b) Nusselt number versus Reynolds number, sample 3.

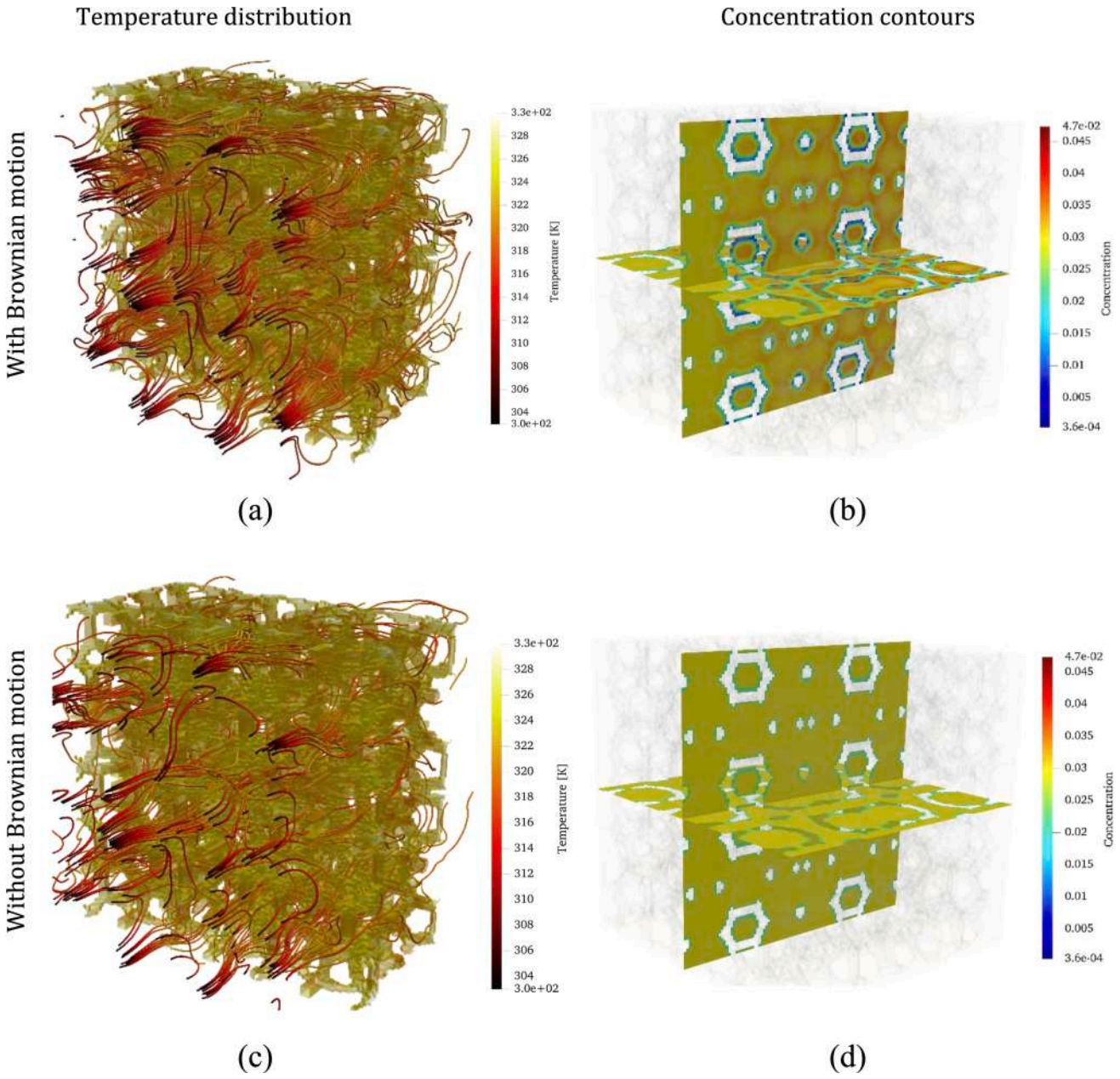

Fig. 9. 3D contours for sample 3 representing temperature distribution and nanoparticle concentration.

energy equations are presented as follows:

Continuity:

$$\nabla.\boldsymbol{V} = 0 \tag{1}$$

Momentum:

$$\rho_{nf}(\boldsymbol{V}.\nabla)\boldsymbol{V} = -\nabla p + \nabla.(\mu_{nf}\nabla\boldsymbol{V}) \tag{2}$$

Nanoparticle distribution:

$$(\boldsymbol{V}.\nabla\varphi) = \frac{1}{\rho_{nf}}\nabla.(\boldsymbol{J_p}) \tag{3}$$

By neglecting thermophoretic effects, only the Brownian force ($\boldsymbol{J_B}$) remains, and we have:

$$\boldsymbol{J_p} = \boldsymbol{J_B} = -\rho_{np}D_B\nabla\varphi \tag{4}$$

In this equation $k_B$is 1.38066×10^{-23} Jk^{-1}. Mass flux includes forces such as Brownian motion, which depends on the density of nanoparticles ρ_{np}. Also, the D_B is estimated from the Einstein-Stokes equation:

$$D_B = \frac{k_B T}{3\pi\mu_f d_{np}} \tag{5}$$

Substituting Eqs. (4), and (5) in Eq. (3), the nanoparticle distribution equation becomes as follows:

$$(\boldsymbol{V}.\nabla\varphi) = -\nabla.(D_B\nabla\varphi) \tag{6}$$

Energy:

$$(\rho C_p)_{nf}(\boldsymbol{V}.\nabla T) = \nabla.(k_{nf}\nabla T) - (C_p)_{np}\boldsymbol{J_p}.\nabla T \tag{7}$$

In the energy equation, the subscript *np* indicates the nanoparticle properties.

2.4. Nanofluid properties and boundary conditions

Different models have been proposed to calculate nanofluid's

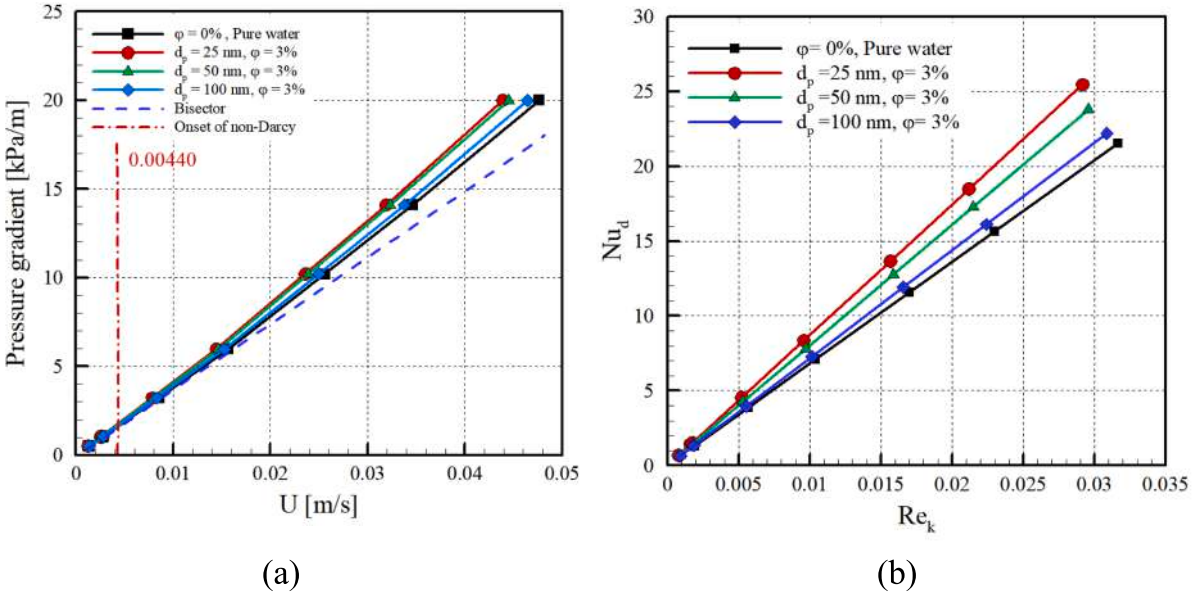

Fig. 10. Nanoparticle diameter effects on a) pressure gradient as a function of the Darcy velocity; b) Nusselt number as a function of Reynolds number, for sample 3.

thermophysical properties. Gupta et al. [69] had collected various models to represent the thermodynamic properties of nanofluids. Nanofluid properties can be obtained by the thermophysical properties of the nanoparticles and base fluid, as follows [70].

$$\rho_{nf} = (1-\varphi)\rho_f + \varphi\rho_{nf} \tag{8}$$

$$(\rho C_p)_{nf} = (1-\varphi)(\rho C_p)_f + \varphi(\rho C_p)_{np} \tag{9}$$

Brinkman's model was developed from the Einstein formula for spherical nanoparticles and moderate particle concentration to calculate the viscosity of the nanofluid, as follows [71]:

$$\mu_{nf} = \frac{\mu_f}{(1-\varphi)^{2.5}} \tag{10}$$

Many relations have been introduced to determine the thermal conductivity of nanofluid [72-74]. The Hamilton-Crosser method is a well-known relation for calculating nanofluid thermal conductivity [75]. This model was developed for spherical nanoparticles and is valid for alumina nanoparticles:

$$\frac{k_{nf}}{k_f} = \frac{k_{np} + 2k_f + 2\varphi(k_{np} - k_{nf})}{k_{np} + 2k_f - \varphi(k_{np} - k_{nf})} \tag{11}$$

2.5. Darcy's law and Forchheimer's relation

Based on the Darcy's law, the pressure gradient in porous media is calculated as follows:

$$-\nabla p = \frac{\mu}{\boldsymbol{K}_D}\boldsymbol{U} \tag{12}$$

Darcy's law is valid for low Reynolds numbers. Hence for higher Reynolds values, the non-Darcy relation proposed by Forchheimer can be implemented.

$$-\nabla p = \frac{\mu}{\boldsymbol{K}_F}\boldsymbol{U} + \rho\beta_F|\boldsymbol{U}|\boldsymbol{U} \tag{13}$$

The permeability terms in Darcy and Forchheimer laws are slightly different [76].

2.6. Non-dimensional parameters

The overall heat transfer coefficient is obtained as follows [64]:

$$h = \frac{q''}{(T_{w,i} - T_{in})} \tag{14}$$

$T_{w,i}$ is defined as follows [64]:

$$T_{w,i} = \frac{(T_w)_{inlet} + (T_w)_{outlet}}{2} \tag{15}$$

The Nusselt number can be calculated by using Eq. (16) [64]:

$$Nu_d = \frac{hd_p}{k_{nf}} \tag{16}$$

The Reynolds number is based on the square root of Darcy permeability, and is defined as follows [77]:

$$Re_k = \frac{\rho U\sqrt{k_D}}{\mu_{nf}} \tag{17}$$

where $\sqrt{k_D}$ indicates the Brinkman screening length [78].

3. Numerical solver and grid independence

3.1. Solver settings

In this research, the governing equations and boundary conditions are solved using object-oriented C++ programming with a FVM, using the OpenFOAM library [79]. The SIMPLE algorithm is utilized for the coupling of velocity and pressure. For discretization of the diffusion and convection terms, the second-order central and the upwind schemes are utilized, respectively. To achieve convergence, the residuals should meet the minimum value of 10^{-7}.

3.2. Mesh refinement study

In this section, to check the independence of results from the computational grid, a mesh refinement analysis is performed for sample 3. The pressure gradient is 20 Pa/m. The values of the overall Nusselt number and the permeability for computational grids from 60^3 to 180^3 are compared in Fig. 3. As can be seen, the grid with 120^3 cells could provide the Nusselt number with only 0.04% difference from the most refined grid. On the other hand, only 0.37% difference exists between the results of this grid and the finest one. Table 4 compares the results of

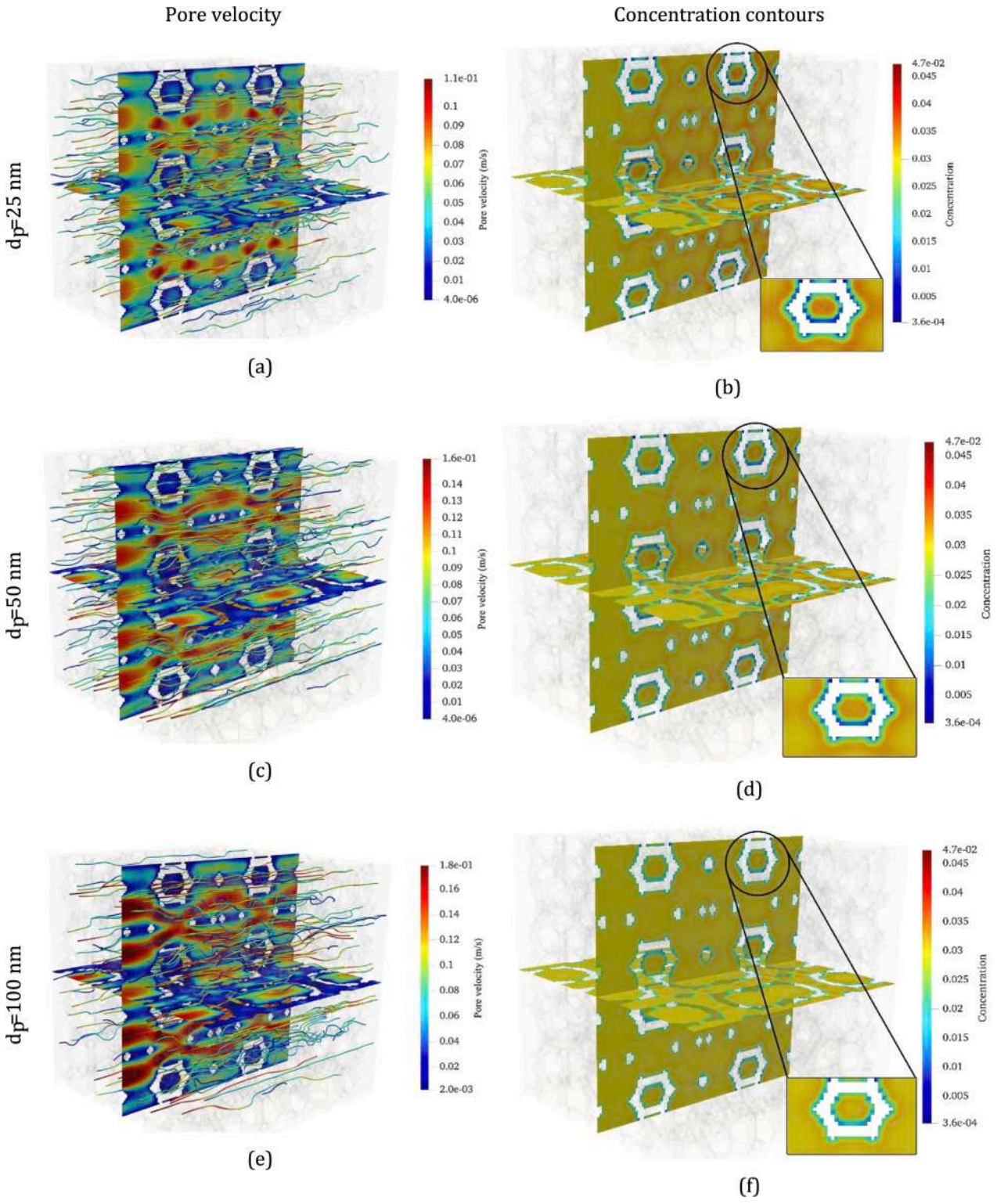

Fig. 11. The pore velocity magnitude, and concentration distributions contours for sample 3 with different nanoparticle diameters (d_p = 25, 50, 100 nm), for the nanofluid concentration of 3% and pressure gradient 20 [kPa/m].

different grids for the three samples of OCMF. For further numerical simulations, the grids for samples 1, 2, and 3 are 180^3, 140^3, and 120^3, respectively.

3.3. Validation

For the validation of the numerical solver, nanofluid flow and heat transfer through the microchannel is simulated by the pore-scale approach. The effects of Brownian, thermophoretic, and lift forces are considered in this study (as depicted in Fig. 4). The results are in close agreement with those of Sharaf et al. [80], with less than 1% deviation.

Sharaf et al. [80] investigated particle migration of alumina nanofluid and its heat transfer by an Eulerian-Lagrangian method. As illustrated in Fig. 5, the non-dimensional velocity (for Re = 16) across the

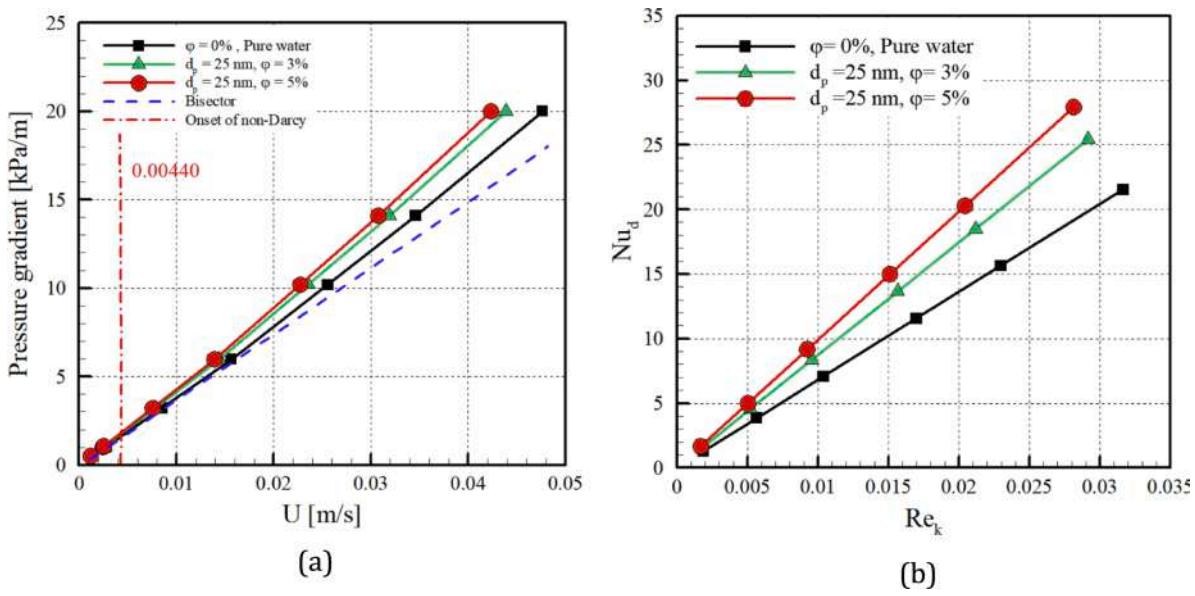

Fig. 12. Nanoparticles' concentration effects on a) pressure gradient as a function of the Darcy velocity; b) Nusselt number as a function of the Reynolds number, for sample 3.

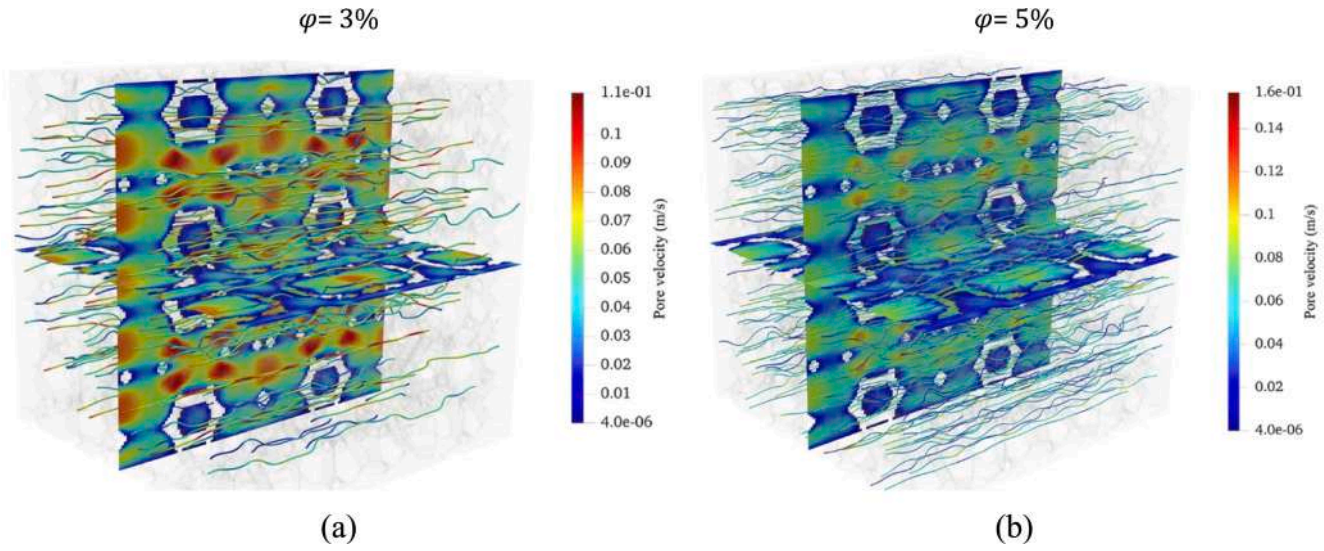

Fig. 13. The pore velocity magnitude contours for sample 3 with different nanoparticle concentrations (φ = 3%, 5%), for nanofluid diameter of 25 nm and pressure gradient of 20 [kPa/m].

outlet of the microchannel height is presented. Also, Fig. 6 illustrates the non-dimensional temperature on horizontal mid-line along the microchannel length for $Re = 4$ and $Re = 16$. Accordingly, the results are in close agreement (less than 1% difference) with those of Yang and Lai [81], and Sharaf et al. [80].

Moreover, Fig. 7 demonstrates the effect of the Brownian motion force on the concentration profile of nanoparticles. The difference between these results is less than 1% and the results are validated with the results of Sharaf et al. [80].

4. Results and discussion

The effects of four parameters: 1) Brownian motion, 2) nanoparticle diameter, 3) nanofluid volume fraction, and 4) the pore density of the metal foam, on hydrodynamics and heat transfer of nanofluid flow, are presented in this section.

4.1. Brownian motion analysis

The collision of fluid molecules and solid particles cause the Brownian motion, which is the random movement of particles in the fluid. In nanofluids, heat and mass transfer can be enhanced considerably because of the diffusion caused by the Brownian motion of particles in the fluid. In this part of the simulation, the effects of the Brownian force on heat transfer coefficient and pressure drop in Darcy and non-Darcy regimes are investigated. Nanoparticles are usually produced with a diameter between 25 and 100 nm. For laminar flows, a nanofluid concentration of about 1–5% is common, and the volume fraction of 3% is more traditional. Since the Brownian motion is more dominant in lower nanoparticles' diameter, it has been assumed that particle diameter has a constant value of 25 nm and the nanofluid volume fraction is 3%. Other volume fractions and nanoparticles' diameters will be tested in the subsequent sections.

Fig. 8 (a) and (b) depict the fluid pressure gradient as a function of

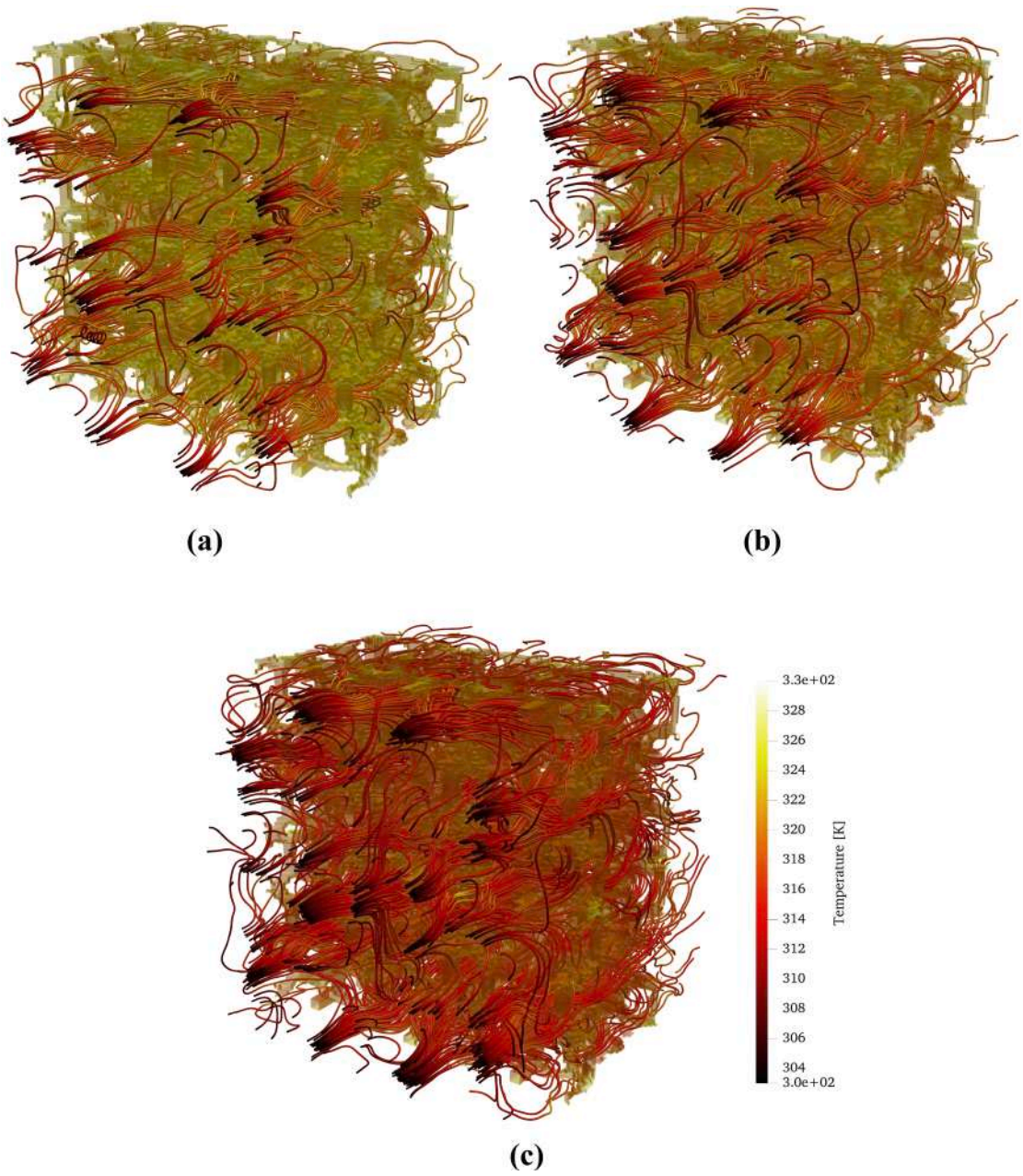

Fig. 14. 3D contours of temperature distribution in a section of metal foams and temperature values on flow streamlines. a) Sample 1 ($Re_k = 0.0207$), b) Sample 2 ($Re_k = 0.0209$), and c) Sample 3 ($Re_k = 0.0211$).

the Darcy velocity and Nusselt versus Reynold number for the pure water and nanofluid (with and without Brownian effects), respectively. Increasing the velocity (or Reynolds number) can increase the pressure gradient and Nusselt number. Comparing the pure fluid and two nanofluid cases (with and without Brownian motion) indicate minor differences in the Darcy regime. However, increasing the velocity (or Re_k) makes the difference between the studied cases more significant. Comparing the pressure gradient and Nu_d reveals that the role of Brownian motion in the heat transfer is more evident than its role in the pressure loss. In the Darcy regime, the Brownian motion has a negligible effect on the pressure drop, while its role becomes significant in the non-Darcy regime. Increasing flow velocity can increase the concentration gradient with subsequent increment in Brownian diffusion. Comparing the pure fluid with the nanofluid without Brownian effects at constant velocity (and Re_k) shows a minor increment in the pressure gradient and Nu_d. While when the Brownian force is active, it has a more significant effect on the Nu_d, and pressure gradient. Applying nanoparticles in pure water can increase the base fluid thermal conductivity and heat transfer. However, the Brownian diffusion of nanoparticles can improve heat transfer even more. We can observe that the Brownian motion effects on heat transfer are significant. The trend of these results are consistent with those obtained by Amani et al. [82] for flows in a channel.

Fig. 9 (a) and (C) exhibit the role of the Brownian motion on temperature distribution contours in the fluid zone for Sample 3. In the sample with Brownian motion, enhancement of nanoparticles' diffusion improves the heat transfer. Also, the flow mixing (as is appeared by the tortuosity of streamlines) is higher in the sample with Brownian motion than in the sample without Brownian effects. Fig. 9 (b) and (d) demonstrate the effect of the Brownian motion on concentration distribution contours. As can be observed in concentration contours, in the sample considering Brownian motion, the random movement of nanoparticles increases, and particles' accumulation near the walls are more

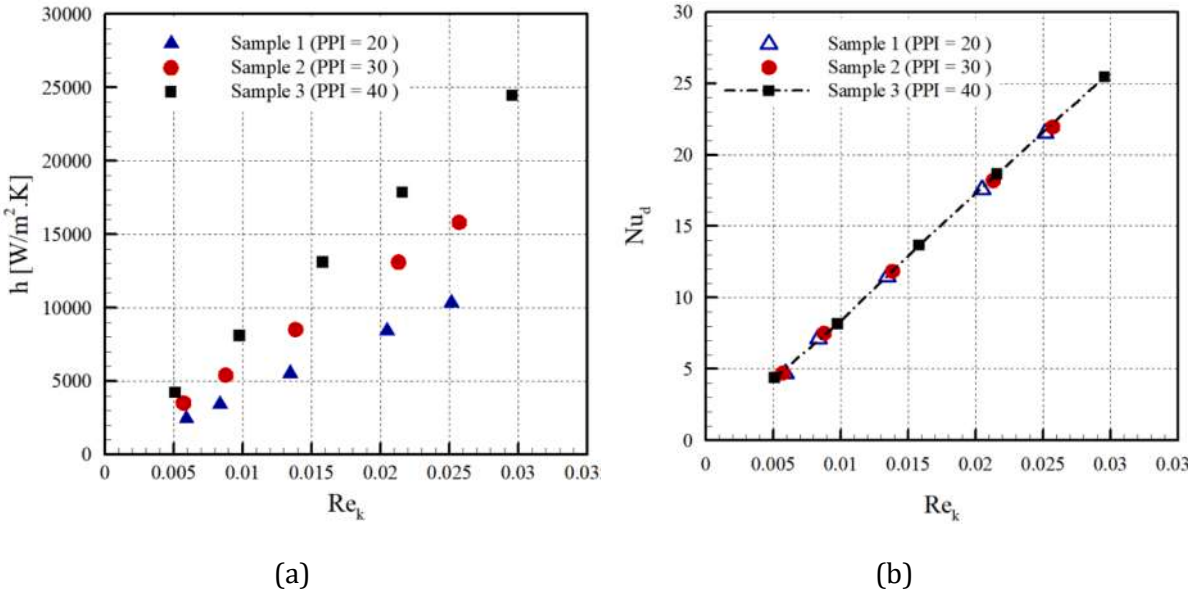

Fig. 15. Variation of a) heat transfer coefficient and b) Nusselt number as a function of Reynolds number for three metal foam samples with the same particle diameter of 25 nm and a concentration of 3%.

significant. Application of a porous medium could enhance the fluid–solid contact. Accordingly, nanoparticles' concentration increase in the vicinity of the solid walls (with the no-slip boundary condition), in the presence of Brownian motion, with subsequent increment in the gradient of nanofluid concentration. The fact that can remarkably increase the Brownian diffusion role in the heat transfer.

4.2. Nanoparticle diameter analysis

This section investigates the effect of nanoparticle diameter on pressure drop and heat transfer. Results are presented in Fig. 10 for Sample 3, considering three different particle diameters, 20, 50, and 100 nm. As expected from Eq. (5), the Brownian force is inversely related to the diameter of the nanoparticles. Hence with the increment in particle diameter, the random motion of nanoparticles decreases for the same particle concentration, which reduces the Brownian force. Therefore, decreasing the particle diameter will increase the Nusselt number and pressure drop. These changes are more noticeable in the non-Darcy region. For instance, by increasing the particle diameter from 25 nm to 100 nm, the Nusselt number enhances less than 1% in the Darcy region and by up to 35% in the non-Darcy region. Additionally, the pressure gradient enhances less than 1% in the Darcy region and up to 28% in the non-Darcy region. The trend of the results reported in this study are consistent with those of Fani et al. [83], who studied Brownian effects in a microchannel.

Decreasing the nanoparticle diameter has two different effects on diffusion motions. From one side the fluid viscosity will decrease that can reduce the shear stress and pressure losses. While on the other side, the Brownian motion will increase that can increase the pressure drop. It seems that by decreasing d_p from 50 nm to 25 nm, these two mechanisms will neutralize each other. Hence, it can be seen that the pressure gradient results of d_p = 25 nm and 50 nm are very close to each other.

Fig. 11 (a), (c), and (e) show the velocity contours and streamlines for sample 3, considering different particle diameters. Due to the effect of Brownian force and its relation with nanoparticle diameter, comparisons between the results of different diameters show that the case with a lower particle diameter has more significant diffusive movement, reducing the flowing velocity. The average Darcy velocity of the case with 100 nm nanoparticles is 6% higher than that of the case with 25 nm nanoparticles. Fig. 11 (b), (d), and (f) illustrate the concentration distribution contours for sample 3 regarding different particle diameters. It has been shown that due to the significant effect of Brownian motion, with nanoparticle diameter reduction, the concentration of nanoparticles around the pores rises. Application of a porous OCF can substantially increase the fluid-solid contact surface. As can be seen in these figures, the gradient of nanofluid concentration near the walls will increase with reducing the nanoparticles' diameter. The fact that can boost the Brownian heat transfer. Hence, we should expect to have a more evident role of Brownian diffusive heat transfer in a porous medium with increased contact surface.

4.3. Effect of nanofluid volume fraction

Based on Eq. (10), the nanofluid concentration has an exponential relationship with viscosity; accordingly, the viscosity will increase with the rise of the nanoparticles' concentration. The fact that can adversely affect the heat transfer and flow velocity. On the other side, by enhancing the nanoparticle concentration, the nanofluid thermal conductivity and the collision between the nanoparticles will be intensified, and this causes an increase in Brownian diffusivity with subsequent heat transfer enhancement. In this section, nanoparticle concentrations of 0%, 3%, and 5% are considered to be studied for foam sample 3. Fig. 12 (a) demonstrates the effects of different concentrations on the pressure gradient versus the Darcy velocity. Also, Fig. 12 (b) depicts the effect of various nanofluid concentrations on Nu_d in different Re_k values. As was observed in the previous section, these effects are more noticeable in the non-Darcy region. For instance, by increasing the nanofluid volume fraction from 3% to 5%, the Nusselt number enhances by less than 1% in the Darcy region and by up to 33% in the non-Darcy region. Additionally, the pressure gradient enhances by less than 1% in the Darcy region and up to 30% in the non-Darcy region. The nanofluid concentration increment can increase the heat transfer rate because of an increase in pressure losses. A remarkable increase in Nu_d is observed by the rise of the volume fraction from 0 to 3%. The further increase from 3% to 5% has a lower impact on Nu_d, reflecting viscosity increment's adverse effect due to the volume fraction increase. The trend of these results agree with those obtained by Amani et al. [82] in a microchannel.

Fig. 13 (a) and (b) demonstrate the influence of nanofluid volume fraction on the velocity contours and streamlines for sample 3. The increased volume fraction led to higher viscosity and higher Brownian

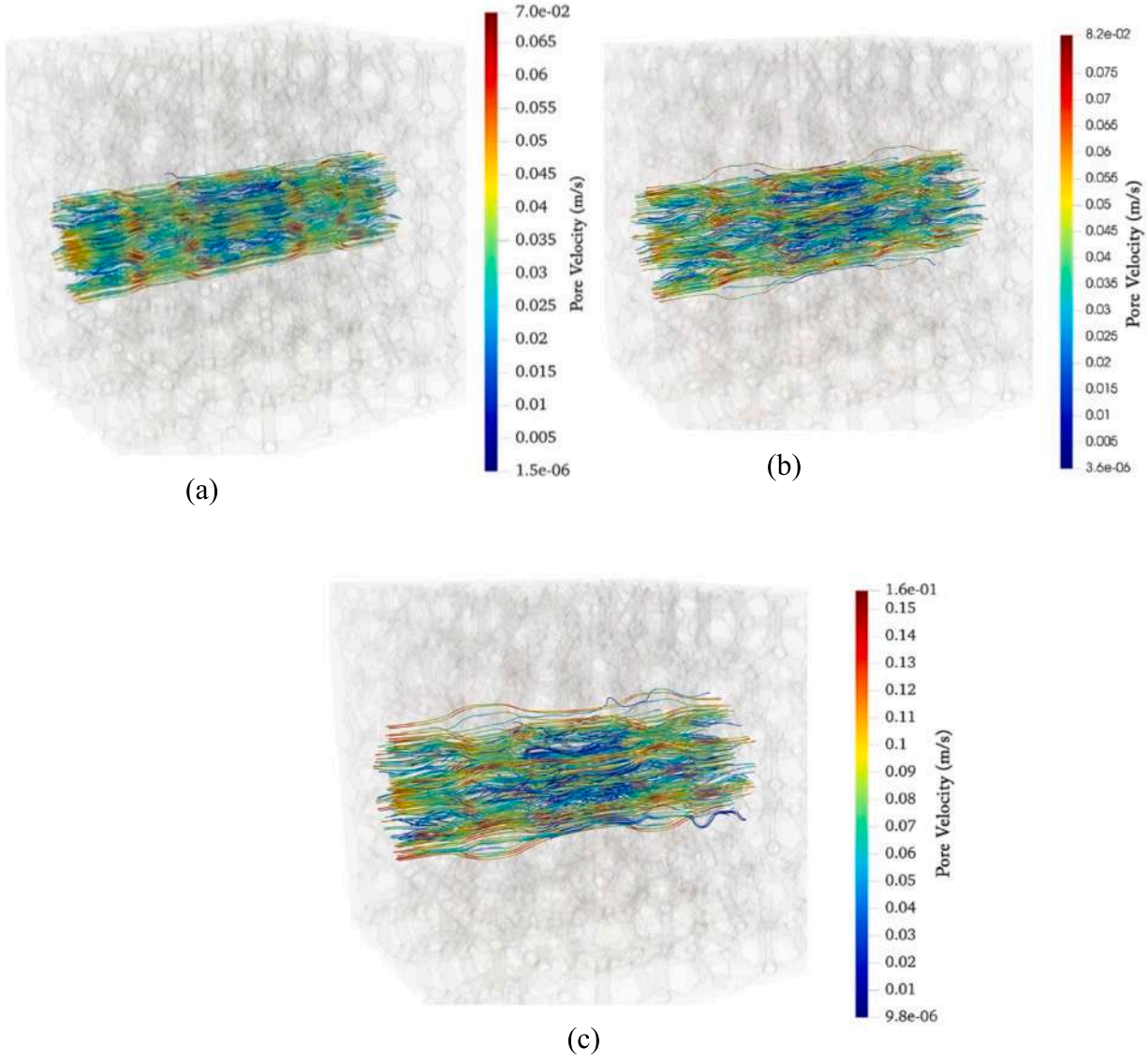

Fig. 16. Fluid flow pattern along the x-axis and 3D contours temperature values on flow streamlines presented for samples1, 2, and 3 of metal foam, shown in (a), (b), and (c), respectively.

effects that can adversely affect the fluid velocity. Obviously, the volume fraction increase reduces the bulk fluid's velocity.

4.4. Pore density analysis

The pore density of the OCF can remarkably affect the flow mixing and subsequently influence the heat transfer rate. In this section, the effect of geometric parameters on the heat transfer of flow in three OCMF samples is reported. In Fig. 14, temperature distribution contours for the three samples are represented. The metal foam has more ligaments and fluid zone contact area per unit volume in samples with smaller pores. Therefore, the solid zone transfers more heat flux to the system due to the high conductivity coefficient in metal foams, and hence the temperature magnitudes reduce in the fluid zone. On the other hand, flow patterns in samples with higher pore density are more complex, which improves the heat transfer capacity of the system. The results exhibit that in sample 3, with higher pore density, the magnitude of the temperature is lower, and the system transfers heat more than in sample 2. Another notable fact is that the Reynolds number value of sample 3 compared to sample 2 is up to 8% higher.

Another important mechanism of heat transfer in porous media in presence of Brownian motion, is the enhanced fluid–solid contact and its role on improved diffusive Brownian heat transfer. As was observed in sections 4.1 and 4.2, the nanofluid concentration around the solid ligaments is higher than other regions. Concentration gradient can magnify the Brownian heat transfer. As the consequence, irrespective to the improved heat transfer surface, we should expect to have a higher heat transfer rate in a porous medium due to the improved Brownian diffusive heat transfer around the solid walls, as is caused by the nanofluid concentration gradient.

Fig. 15 (a) depicts the overall heat transfer coefficient for different Re_k values. The results show that increasing pore density leads to a significant rise in the overall heat transfer coefficient. For instance, in the approximately same value of Reynolds number (Re_k = 0.0207 in sample 1, and Re_k = 0.0211 in sample 3), the overall heat transfer coefficient for samples 1, and 3 are 11,910 $W/(m^2K)$, and 17,175 $W/(m^2K)$, respectively. The trend of these results are consistent with the experimental results of Beer et al. [84] for a pure fluid flow through porous media.

Fig. 15 (b) exhibits the global Nusselt number of different metal foam samples. The results demonstrate that for various samples with the same diameter and concentration of nanoparticles, Nu_d is a function of the

Reynolds number. As a result, Nu_d is independent of pore diameter, which agrees with the published data in the literature [64].

The flow patterns of various OCMF samples are shown in Fig. 16 to compare the influence of pore density on the velocity and complexity (or tortuosity) of flow in different samples. The investigation of flow at the pore-scale simulation depicts that the tortuosity of the flow pattern in the voids in the high porosity samples is less than the predicted flow patterns of the low-porosity rocks. Compring a high-porosity foam (with a porosity of higher than 0.8) against a low-porosity rock (with a porosity of lower than 0.25) reveals that the high-porosity foam could provide more space for flow and reduces the tortuosity of steamlines. While, the porosity of rocks are remarkably lower than foams which can increase the flow tortuosity and complexity. These results are coherent with the research results by Poureslami et al. [64].

5. Conclusions and future directions

The present work investigated pore-scale analysis of two-phase nanofluid heat transfer and flow in open-cell metal foams (OCMFs) by considering the effect of Brownian motion in the different values of Reynolds number by Darcy and non-Darcy flow regimes. The finite volume method (FVM) is implemented to resolve the problem, and the three-dimensional (3D) numerical code is developed in the open-source library of OpenFOAM. Weaire–Phelan (WP) foam structures with a constant porosity (0.86) and various pore sizes are constructed to perform direct numerical simulation (DNS) studies. The nanofluid flow is simulated with the Buongiorno's model. The effect of Brownian motion, nanoparticle diameter, particle concentration, and the pore density of open-cell foams (OCFs) on hydrodynamics and heat transfer have been analyzed. The results obtained that:

- Brownian motion reduces the average Darcy velocity in the Darcy and non-Darcy flow regimes. On the other hand, the Nusselt number and the heat transfer coefficient increase.
- Increasing the diameter of nanoparticles reduces the particles' random motion and hence, the Brownian motion force.
- Increasing the nanoparticles' concentration rises the viscosity. According to the Darcy-Forchhiemer equations, with a constant pressure drop and constant geometric parameters, this reduces the flow velocity. Furthermore, increasing the concentration of nanoparticles increases the heat transfer coefficient and Nusselt number.
- With a constant porosity, the Nusselt number based on pore diameter (Nu_d) is a function of the Reynolds number (Re_k) and independent of pore diameter.
- An important mechanism of improved heat transfer of nanofluid flow in porous media is the concentration gradient around solid walls that can boost the Brownian diffusive heat transfer.

Future studies suggest extending the solver for investigating other forces such as thermophoresis, the drag force, Saffman lift, and van der Waals effects in OCMF samples. Also, the deposition of nanoparticles on the surface of porous media can be the subject of future studies.

CRediT authorship contribution statement

Hamidreza Khoshtarash: Methodology, Software, Validation, Visualization, Writing – original draft. **Majid Siavashi:** Conceptualization, Investigation, Resources, Data curation, Writing – review & editing, Supervision, Project administration. **Milad Ramezanpour:** Formal analysis, Methodology, Software, Visualization. **Martin J. Blunt:** Formal analysis, Methodology, Software, Visualization.

Declaration of Competing Interest

The authors declare that they have no known competing financial interests or personal relationships that could have appeared to influence the work reported in this paper.

Data availability

Data will be made available on request.

Acknowledgment

The authors are grateful for the financial support of the Iran National Science Foundation (INSF) [grant number: 8153].

References

[1] M. Lysyy, G. Ersland, M. Fernø, Pore-scale dynamics for underground porous media hydrogen storage, Adv. Water Resour. 163 (2022), 104167, https://doi.org/10.1016/j.advwatres.2022.104167.
[2] A. Banerjee, D. Paul, Developments and applications of porous medium combustion: A recent review, Energy 221 (2021), 119868, https://doi.org/10.1016/j.energy.2021.119868.
[3] Y. Cao, M. Bezaatpour, H. Ghaebi, Heat transfer and thermodynamic analysis of individual and simultaneous effects of revolution, microporous media, magnetic inductor, and nanoparticles in concentrating solar collectors, Int. Commun. Heat Mass Transf. 129 (2021), 105687, https://doi.org/10.1016/j.icheatmasstransfer.2021.105687.
[4] Z. Wang, J.-M. Pereira, E. Sauret, S.A. Aryana, Z. Shi, Y. Gan, A pore-resolved interface tracking algorithm for simulating multiphase flow in arbitrarily structured porous media, Adv. Water Resour. 162 (2022), 104152, https://doi.org/10.1016/j.advwatres.2022.104152.
[5] Y. Zhuang, Z. Liu, W. Xu, Effects of gradient porous metal foam on the melting performance and energy storage of composite phase change materials subjected to an internal heater: A numerical study and PIV experimental validation, Int. J. Heat Mass Transf. 183 (2022), 122081, https://doi.org/10.1016/j.ijheatmasstransfer.2021.122081.
[6] H. Zhang, Y. Shuai, Y. Yuan, B. Guene Lougou, B. Jiang, F. Wang, Z. Cheng, Thermal-chemical reaction characteristics of Ni/Al2O3 catalytic porous material filled solar reactor for dry reforming of methane process, Appl. Therm. Eng. 180 (2020), 115901, https://doi.org/10.1016/j.applthermaleng.2020.115901.
[7] M. Liu, J. Waugh, S.K. Babu, J.S. Spendelow, Q. Kang, Numerical modeling of ion transport and adsorption in porous media: A pore-scale study for capacitive deionization desalination, Desalination 526 (2022), 115520, https://doi.org/10.1016/j.desal.2021.115520.
[8] D. Zhang, T. Liu, V. Prigiobbe, Enhanced solute transport in porous media due to pH-dependent adsorption and transverse dispersion, Adv. Water Resour. 164 (2022), 104195, https://doi.org/10.1016/j.advwatres.2022.104195.
[9] A. Banerjee, S. Pasupuleti, K. Mondal, M.M. Nezhad, Application of data driven machine learning approach for modelling of non-linear filtration through granular porous media, Int. J. Heat Mass Transf. 179 (2021), 121650, https://doi.org/10.1016/j.ijheatmasstransfer.2021.121650.
[10] X. Zhang, X. Ma, S. Shuai, Y. Qin, J. Yang, Effect of micro-porous layer on PEM fuel cells performance: Considering the spatially variable properties, Int. J. Heat Mass Transf. 178 (2021), 121592, https://doi.org/10.1016/j.ijheatmasstransfer.2021.121592.
[11] H. Pourrahmani, J. Van herle, Evaluation Criterion of Proton Exchange Membrane (ECPEM) fuel cells considering inserted porous media inside the gas flow channel, Appl. Therm. Eng. 203 (2022) 117952. https://doi.org/10.1016/j.applthermaleng.2021.117952.
[12] K. Rajesh, S. Ghosh, A. Islam, M.K. Rangaswamy, S. Haldar, P. Roy, A.K. Keshri, D. Lahiri, Multilayered porous hydroxyapatite coating on Ti6Al4V implant with enhanced drug delivery and antimicrobial properties, J. Drug Deliv. Sci. Technol. 70 (2022), 103155, https://doi.org/10.1016/j.jddst.2022.103155.
[13] N. Dukhan, A.A. Hmad, Thermal management of fuel-cell stacks using air flow in open-cell metal foam, Int. J. Therm. Sci. 172 (2022), 107370, https://doi.org/10.1016/j.ijthermalsci.2021.107370.
[14] P.H. Jadhav, G. n.,, Optimum design of heat exchanging device for efficient heat absorption using high porosity metal foams, Int. Commun. Heat Mass Transf. 126 (2021), 105475, https://doi.org/10.1016/j.icheatmasstransfer.2021.105475.
[15] P. Samudre, S.V. Kailas, Thermal performance enhancement in open-pore metal foam and foam-fin heat sinks for electronics cooling, Appl. Therm. Eng. 205 (2022), 117885, https://doi.org/10.1016/j.applthermaleng.2021.117885.
[16] M. Valizade, M.M. Heyhat, M. Maerefat, Experimental study of the thermal behavior of direct absorption parabolic trough collector by applying copper metal foam as volumetric solar absorption, Renew. Energy 145 (2020) 261–269, https://doi.org/10.1016/j.renene.2019.05.112.
[17] J.S. Baruah, V. Athawale, P. Rath, A. Bhattacharya, Melting and energy storage characteristics of macro-encapsulated PCM-metal foam system, Int. J. Heat Mass Transf. 182 (2022), 121993, https://doi.org/10.1016/j.ijheatmasstransfer.2021.121993.
[18] J. Guo, Z. Du, G. Liu, X. Yang, M.-J. Li, Compression effect of metal foam on melting phase change in a shell-and-tube unit, Appl. Therm. Eng. 206 (2022), 118124, https://doi.org/10.1016/j.applthermaleng.2022.118124.
[19] C. Italiano, G. Drago Ferrante, L. Pino, M. Laganà, M. Ferraro, V. Antonucci, A. Vita, Silicon carbide and alumina open-cell foams activated by Ni/CeO2-ZrO2

catalyst for CO2 methanation in a heat-exchanger reactor, Chem. Eng. J. 434 (2022), 134685, https://doi.org/10.1016/j.cej.2022.134685.
[20] X. Yang, J. Guo, B. Yang, H. Cheng, P. Wei, Y.-L. He, Design of non-uniformly distributed annular fins for a shell-and-tube thermal energy storage unit, Appl. Energy 279 (2020), 115772, https://doi.org/10.1016/j.apenergy.2020.115772.
[21] X. Yang, P. Wei, X. Wang, Y.-L. He, Gradient design of pore parameters on the melting process in a thermal energy storage unit filled with open-cell metal foam, Appl. Energy 268 (2020), 115019, https://doi.org/10.1016/j.apenergy.2020.115019.
[22] T. Busser, M. Serres, R. Philippe, V. Vidal, Hydrodynamics of gas-liquid co-current flow through a thin sheet of highly porous open cell solid foam, Chem. Eng. Sci. 226 (2020), 115811, https://doi.org/10.1016/j.ces.2020.115811.
[23] M.J. Blunt, B. Bijeljic, H. Dong, O. Gharbi, S. Iglauer, P. Mostaghimi, A. Paluszny, C. Pentland, Pore-scale imaging and modelling, Adv. Water Resour. 51 (2013) 197–216, https://doi.org/10.1016/j.advwatres.2012.03.003.
[24] A.Q. Raeini, L.M. Giudici, M.J. Blunt, B. Bijeljic, Generalized network modelling of two-phase flow in a water-wet and mixed-wet reservoir sandstone: Uncertainty and validation with experimental data, Adv. Water Resour. 164 (2022) 104194.
[25] M. Ramezanpour, M. Siavashi, A.Q. Raeini, M.J. Blunt, Pore-scale simulation of nanoparticle transport and deposition in a microchannel using a Lagrangian approach, J. Mol. Liq. 355 (2022), 118948, https://doi.org/10.1016/j.molliq.2022.118948.
[26] A. Kopanidis, A. Theodorakakos, E. Gavaises, D. Bouris, 3D numerical simulation of flow and conjugate heat transfer through a pore scale model of high porosity open cell metal foam, Int. J. Heat Mass Transf. 53 (2010) 2539–2550, https://doi.org/10.1016/j.ijheatmasstransfer.2009.12.067.
[27] H. Moghimi, M. Siavashi, M. Mousavi Nezhad, A. Guadagnini, Pore-scale computational analyses of non-Darcy flow through highly porous structures with various degrees of geometrical complexity, Sustain. Energy Technol. Assess. 52 (2022), 102048, https://doi.org/10.1016/j.seta.2022.102048.
[28] Y. Yao, H. Wu, Z. Liu, Pore Scale Investigation of Heat Conduction of High Porosity Open-Cell Metal Foam/Paraffin Composite, J. Heat Transf. 139 (2017), https://doi.org/10.1115/1.4036526.
[29] T. G, G. N, Numerical study on maximizing heat transfer and minimizing flow resistance behavior of metal foams owing to their structural properties, Int. J. Therm. Sci. 159 (2021) 106617.
[30] W. Jamshed, A.K. Alanazi, S. Suzilliana Putri Mohamed Isa, R. Banerjee, M.R. Eid, K. Sooppy Nisar, H. Alshahrei, M. Goodarzi, Thermal efficiency enhancement of solar aircraft by utilizing unsteady hybrid nanofluid: A single-phase optimized entropy analysis, Sustain. Energy Technol. Assess. 52 (2022) 101898.
[31] A. Izadi, M. Siavashi, H. Rasam, Q. Xiong, MHD enhanced nanofluid mediated heat transfer in porous metal for CPU cooling, Appl. Therm. Eng. 168 (2020), 114843, https://doi.org/10.1016/j.applthermaleng.2019.114843.
[32] S. Sharifi, M.R. Aligoodarz, A. Rahbari, Thermohydraulic performance of Al2O3-water nanofluid during single-phase flow and two-phase subcooled flow boiling, Int. J. Therm. Sci. 179 (2022), 107605, https://doi.org/10.1016/j.ijthermalsci.2022.107605.
[33] W. Cai, D. Toghraie, A. Shahsavar, P. Barnoon, A. Khan, M. Heydari Beni, J. Eskandari Jam, Eulerian-Lagrangian investigation of nanoparticle migration in the heat sink by considering different block shape effects, Appl. Therm. Eng. 199 (2021), 117593, https://doi.org/10.1016/j.applthermaleng.2021.117593.
[34] M. Jamshidmofid, M. Bahiraei, Hydrothermal performance of single and hybrid nanofluids in Left-Right and Up-Down wavy microchannels using two-phase mixture approach, Int. Commun. Heat Mass Transf. 129 (2021), 105752, https://doi.org/10.1016/j.icheatmasstransfer.2021.105752.
[35] B. Mahanthesh, S.A. Shehzad, J. Mackolil, N.S. Shashikumar, Heat transfer optimization of hybrid nanomaterial using modified Buongiorno model: A sensitivity analysis, Int. J. Heat Mass Transf. 171 (2021), 121081, https://doi.org/10.1016/j.ijheatmasstransfer.2021.121081.
[36] M. Javed, M. Farooq, Mixed convection and melting rheology in dual stratified Eyring-Powell nanofluid flow over surface of variable thickness: Buongiorno model approach, Int. Commun. Heat Mass Transf. 125 (2021), 105322, https://doi.org/10.1016/j.icheatmasstransfer.2021.105322.
[37] J. Mohebbi Najm Abad, R. Alizadeh, A. Fattahi, M.H. Doranehgard, E. Alhajri, N. Karimi, Analysis of transport processes in a reacting flow of hybrid nanofluid around a bluff-body embedded in porous media using artificial neural network and particle swarm optimization, J. Mol. Liq. 313 (2020) 113492.
[38] A. Baïri, Porous materials saturated with water-copper nanofluid for heat transfer improvement between vertical concentric cones, Int. Commun. Heat Mass Transf. 126 (2021), 105439, https://doi.org/10.1016/j.icheatmasstransfer.2021.105439.
[39] M. Sheikholeslami, A. Zeeshan, Mesoscopic simulation of CuOH2O nanofluid in a porous enclosure with elliptic heat source, Int. J. Hydrog. Energy. 42 (2017) 15393–15402, https://doi.org/10.1016/j.ijhydene.2017.04.276.
[40] H. Fazeli, S. Madani, P. Rahim Mashaei, Nanofluid forced convection in entrance region of a baffled channel considering nanoparticle migration, Appl. Therm. Eng. 106 (2016) 293–306, https://doi.org/10.1016/j.applthermaleng.2016.06.010.
[41] S.E. Ghasemi, A.A. Ranjbar, Effect of using nanofluids on efficiency of parabolic trough collectors in solar thermal electric power plants, Int. J. Hydrog. Energy 42 (2017) 21626–21634, https://doi.org/10.1016/j.ijhydene.2017.07.087.
[42] M.H. Matin, I. Pop, Forced convection heat and mass transfer flow of a nanofluid through a porous channel with a first order chemical reaction on the wall, Int. Commun. Heat Mass Transf. 46 (2013) 134–141, https://doi.org/10.1016/j.icheatmasstransfer.2013.05.001.
[43] C. Dickson, M. Torabi, N. Karimi, First and second law analyses of nanofluid forced convection in a partially-filled porous channel – The effects of local thermal non-equilibrium and internal heat sources, Appl. Therm. Eng. 103 (2016) 459–480, https://doi.org/10.1016/j.applthermaleng.2016.04.095.
[44] Z. Li, P. Barnoon, D. Toghraie, R. Balali Dehkordi, M. Afrand, Mixed convection of non-Newtonian nanofluid in an H-shaped cavity with cooler and heater cylinders filled by a porous material: Two phase approach, Adv. Powder Technol. 30 (2019) 2666–2685, https://doi.org/10.1016/j.apt.2019.08.014.
[45] S.Y. Motlagh, E. Golab, A.N. Sadr, Two-phase modeling of the free convection of nanofluid inside the inclined porous semi-annulus enclosure, Int. J. Mech. Sci. 164 (2019), 105183, https://doi.org/10.1016/j.ijmecsci.2019.105183.
[46] M.A. Sheremet, I. Pop, Effect of local heater size and position on natural convection in a tilted nanofluid porous cavity using LTNE and Buongiorno's models, J. Mol. Liq. 266 (2018) 19–28, https://doi.org/10.1016/j.molliq.2018.06.065.
[47] S. Yekani Motlagh, S. Taghizadeh, H. Soltanipour, Natural convection heat transfer in an inclined square enclosure filled with a porous medium saturated by nanofluid using Buongiorno's mathematical model, Adv. Powder Technol. 27 (2016) 2526–2540, https://doi.org/10.1016/j.apt.2016.09.016.
[48] A. Malvandi, M. Zamani, S.J. Hosseini, S.A. Moshizi, Figure of merit for optimization of nanofluid flow in circular microchannel by adapting nanoparticle migration, Appl. Therm. Eng. 118 (2017) 328–338, https://doi.org/10.1016/j.applthermaleng.2017.02.081.
[49] A. Malvandi, D.D. Ganji, I. Pop, Laminar filmwise condensation of nanofluids over a vertical plate considering nanoparticles migration, Appl. Therm. Eng. 100 (2016) 979–986, https://doi.org/10.1016/j.applthermaleng.2016.02.061.
[50] F. Selimefendigil, H.F. Öztop, Magnetohydrodynamics forced convection of nanofluid in multi-layered U-shaped vented cavity with a porous region considering wall corrugation effects, Int. Commun. Heat Mass Transf. 113 (2020), 104551, https://doi.org/10.1016/j.icheatmasstransfer.2020.104551.
[51] M. Siavashi, H.R. Talesh Bahrami, H. Saffari, Numerical investigation of flow characteristics, heat transfer and entropy generation of nanofluid flow inside an annular pipe partially or completely filled with porous media using two-phase mixture model, Energy 93 (2015) 2451–2466, https://doi.org/10.1016/j.energy.2015.10.100.
[52] M. Sheikholeslami, CuO-water nanofluid free convection in a porous cavity considering Darcy law, Eur. Phys. J. Plus. 132 (2017) 55, https://doi.org/10.1140/epjp/i2017-11330-3.
[53] M.M. Heyhat, M. Valizade, S.h. Abdolahzade, M. Maerefat, Thermal efficiency enhancement of direct absorption parabolic trough solar collector (DAPTSC) by using nanofluid and metal foam, Energy 192 (2020), 116662, https://doi.org/10.1016/j.energy.2019.116662.
[54] M. Hatami, J. Geng, D. Jing, Enhanced efficiency in Concentrated Parabolic Solar Collector (CPSC) with a porous absorber tube filled with metal nanoparticle suspension, Green, Energy Environ. 3 (2018) 129–137, https://doi.org/10.1016/j.gee.2017.12.002.
[55] S. Andarwa, H. Basirat Tabrizi, G. Ahmadi, Effect of correcting near-wall forces on nanoparticle transport in a microchannel, Particuology 16 (2014) 84–90, https://doi.org/10.1016/j.partic.2013.11.007.
[56] S. Andarwa, H.B. Tabrizi, Nanoparticle deposition in transient gaseous microchannel flow considering hindered motion and rarefaction effect, Korean J. Chem. Eng. 34 (2017) 1319–1327, https://doi.org/10.1007/s11814-017-0022-4.
[57] N. Seetha, A. Raoof, M.S. Mohan Kumar, S. Majid Hassanizadeh, Upscaling of nanoparticle transport in porous media under unfavorable conditions: Pore scale to Darcy scale, J. Contam. Hydrol. 200 (2017) 1–14, https://doi.org/10.1016/j.jconhyd.2017.03.002.
[58] W. Kuang, S. Saraji, M. Piri, Pore-Scale Sweep Efficiency Enhancement by Silica-Based Nanofluids in Oil-Wet Sandstone, Energy Fuels 34 (2) (2020) 1297–1308.
[59] A.V. Minakov, D.V. Guzei, M.I. Pryazhnikov, S.A. Filimonov, Y.O. Voronenkova, 3D pore-scale modeling of nanofluids-enhanced oil recovery, Pet. Explor. Dev. 48 (2021) 956–967, https://doi.org/10.1016/S1876-3804(21)60080-0.
[60] B. Zhang, A.I.A. Mohamed, L. Goual, M. Piri, Pore-scale experimental investigation of oil recovery enhancement in oil-wet carbonates using carbonaceous nanofluids, Sci. Rep. 10 (2020) 17539, https://doi.org/10.1038/s41598-020-74450-w.
[61] J. Su, G. Chai, L. Wang, W. Cao, Z. Gu, C. Chen, X.Y. Xu, Pore-scale direct numerical simulation of particle transport in porous media, Chem. Eng. Sci. 199 (2019) 613–627, https://doi.org/10.1016/j.ces.2019.01.033.
[62] E. Sepehri, M. Siavashi, Pore-scale direct numerical simulation of fluid dynamics, conduction and convection heat transfer in open-cell Voronoi porous foams, Int. Commun. Heat Mass Transf. 137 (2022), 106274, https://doi.org/10.1016/j.icheatmasstransfer.2022.106274.
[63] B. Buonomo, A. di Pasqua, O. Manca, S. Nappo, S. Nardini, Entropy generation analysis of laminar forced convection with nanofluids at pore length scale in porous structures with Kelvin cells, Int. Commun. Heat Mass Transf. 132 (2022), 105883, https://doi.org/10.1016/j.icheatmasstransfer.2022.105883.
[64] P. Poureslami, M. Siavashi, H. Moghimi, M. Hosseini, Pore-scale convection-conduction heat transfer and fluid flow in open-cell metal foams: A three-dimensional multiple-relaxation time lattice Boltzmann (MRT-LBM) solution, Int. Commun. Heat Mass Transf. 126 (2021), 105465, https://doi.org/10.1016/j.icheatmasstransfer.2021.105465.
[65] B. Buffel, F. Desplentere, K. Bracke, I. Verpoest, Modelling open cell-foams based on the Weaire-Phelan unit cell with a minimal surface energy approach, Int. J. Solids Struct. 51 (2014) 3461–3470, https://doi.org/10.1016/j.ijsolstr.2014.06.017.
[66] S. Cunsolo, M. Iasiello, M. Oliviero, N. Bianco, W.K.S. Chiu, V. Naso, Lord Kelvin and Weaire-Phelan Foam Models: Heat Transfer and Pressure Drop, J. Heat Transf. 138 (2015), https://doi.org/10.1115/1.4031700.

[67] Z. Guo, C. Zheng, B. Shi, Discrete lattice effects on the forcing term in the lattice Boltzmann method, Phys. Rev. E 65 (2002), 046308, https://doi.org/10.1103/PhysRevE.65.046308.
[68] J. Buongiorno, Convective Transport in Nanofluids, J. Heat Transf. 128 (2005) 240–250, https://doi.org/10.1115/1.2150834.
[69] M. Gupta, V. Singh, R. Kumar, Z. Said, A review on thermophysical properties of nanofluids and heat transfer applications, Renew. Sustain. Energy Rev. 74 (2017) 638–670, https://doi.org/10.1016/j.rser.2017.02.073.
[70] M.U. Sajid, H.M. Ali, Recent advances in application of nanofluids in heat transfer devices: A critical review, Renew. Sustain. Energy Rev. 103 (2019) 556–592, https://doi.org/10.1016/j.rser.2018.12.057.
[71] H.C. Brinkman, The Viscosity of Concentrated Suspensions and Solutions, J. Chem. Phys. 20 (1952) 571–571. https://doi.org/10.1063/1.1700493.
[72] S. Yekani Motlagh, A. Sharifi, M. Ahmadi, H. Badfar, Presentation of new thermal conductivity expression for Al2O3–water and cuo–water nanofluids using gene expression programming (GEP), J. Therm. Anal. Calorim. (2018) 1–12.
[73] Y. Li, Y. Zhai, M. Ma, Z. Xuan, H. Wang, Using molecular dynamics simulations to investigate the effect of the interfacial nanolayer structure on enhancing the viscosity and thermal conductivity of nanofluids, Int. Commun. Heat Mass Transf. 122 (2021), 105181, https://doi.org/10.1016/j.icheatmasstransfer.2021.105181.
[74] T. Ambreen, M.-H. Kim, Influence of particle size on the effective thermal conductivity of nanofluids: A critical review, Appl. Energy. 264 (2020), 114684, https://doi.org/10.1016/j.apenergy.2020.114684.
[75] R.L. Hamilton, O.K. Crosser, Thermal Conductivity of Heterogeneous Two-Component Systems, Ind. Eng. Chem. Fundam. 1 (1962) 187–191, https://doi.org/10.1021/i160003a005.
[76] S.-H. Park, D.-H. Seo, J.H. Jeong, Experimental and numerical analysis of thermal flow in open-cell porous metal during Darcy-Forchheimer transition regime, Appl. Therm. Eng. 181 (2020), 116029, https://doi.org/10.1016/j.applthermaleng.2020.116029.
[77] B.P. Muljadi, M.J. Blunt, A.Q. Raeini, B. Bijeljic, The impact of porous media heterogeneity on non-Darcy flow behaviour from pore-scale simulation, Adv. Water Resour. 95 (2016) 329–340, https://doi.org/10.1016/j.advwatres.2015.05.019.
[78] L. Durlofsky, J.F. Brady, Analysis of the Brinkman equation as a model for flow in porous media, Phys. Fluids 30 (1987) 3329–3341, https://doi.org/10.1063/1.866465.
[79] OpenFOAM Resources | Documentation | OpenFOAM, (n.d.). https://openfoam.org/resources/ (accessed October 22, 2021).
[80] O.Z. Sharaf, A.N. Al-Khateeb, D.C. Kyritsis, E. Abu-Nada, Numerical investigation of nanofluid particle migration and convective heat transfer in microchannels using an Eulerian-Lagrangian approach, J. Fluid Mech. 878 (2019) 62–97, https://doi.org/10.1017/jfm.2019.606.
[81] Y.-T. Yang, F.-H. Lai, Numerical study of flow and heat transfer characteristics of alumina-water nanofluids in a microchannel using the lattice Boltzmann method, Int. Commun. Heat Mass Transf. 38 (2011) 607–614, https://doi.org/10.1016/j.icheatmasstransfer.2011.03.010.
[82] M. Amani, P. Amani, M. Bahiraei, M. Ghalambaz, G. Ahmadi, L.-P. Wang, S. Wongwises, O. Mahian, Latest developments in nanofluid flow and heat transfer between parallel surfaces: A critical review, Adv. Colloid Interface Sci. 294 (2021), 102450, https://doi.org/10.1016/j.cis.2021.102450.
[83] B. Fani, M. Kalteh, A. Abbassi, Investigating the effect of Brownian motion and viscous dissipation on the nanofluid heat transfer in a trapezoidal microchannel heat sink, Adv. Powder Technol. 26 (2015) 83–90, https://doi.org/10.1016/j.apt.2014.08.009.
[84] M. Beer, R. Rybár, M. Kaľavský, Experimental heat transfer analysis of open cell hollow ligament metal foam at low Reynolds number, Measurement 133 (2019) 214–221, https://doi.org/10.1016/j.measurement.2018.10.025.